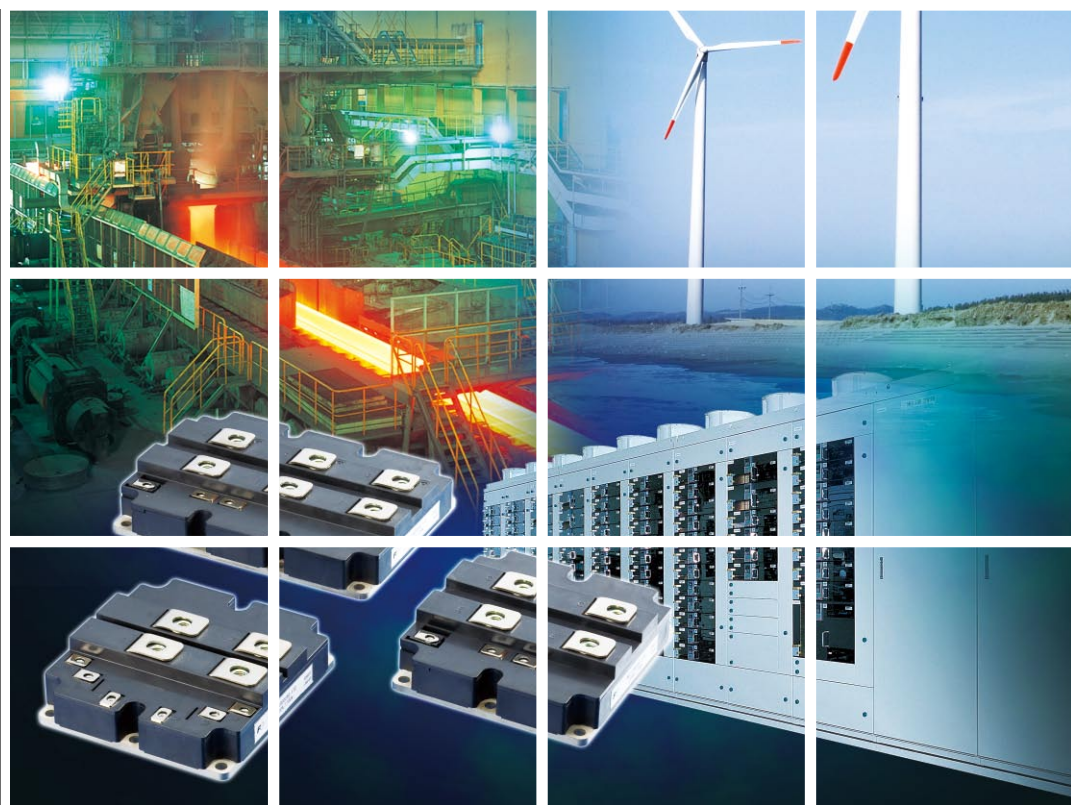


# FUJI ELECTRIC REVIEW

Semiconductors



2009 VOL.55



**Fuji Electric Group**



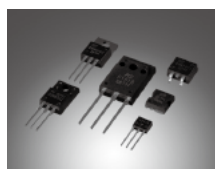
## The seeds of energy savings.

Energy savings has become a vital theme for automobiles, digital household appliances, industrial robots, and all other electric and electronic devices. The key devices to realizing this energy savings are power semiconductors that are built into the power supply unit and that control the supply of electric power. Fuji Electric Device Technology's power semiconductors, through higher efficiency power control and a smaller and lighter-weight package, contribute significantly to energy savings in electric equipment. These are the true seeds of energy savings. Furthermore, Fuji Electric Device Technology is among the first to discontinue the use of substances that burden the environment, and is moving ahead with compliance with all sorts of environmental regulations and aims to achieve a bright future with advanced power semiconductors.



### IGBT modules

Power devices for use in power conversion equipment. Equipped with state-of-the-art chips, these IGBT modules achieve lower loss and higher efficiency, and have been made into a product series.



### Power MOSFETs

With low on-resistance performance, high surge resistance and high-speed switching are possible. Presently being used in a wide range of applications including all types of power supply equipment and battery-powered equipment.

# FUJI ELECTRIC REVIEW

Semiconductors

2

2009 VOL.55

## CONTENTS

|   |    |
|---|----|
| Fuji Electric's Semiconductors: Current Status and Future Outlook               | 42 |
| IGBT Modules for Hybrid Vehicle Motor Driving                                   | 46 |
| High-power IGBT Modules   | 51 |
| 6th Generation Power MOSFET Super FAP-E <sup>3S</sup> Low Q <sub>g</sub> Series | 56 |
| SMD-type Small Atmospheric Pressure Sensor for High-altitude Compensation       | 61 |
| Modeling of Conduction EMI Noise and Technology for Noise Reduction             | 64 |
| Technology for Controlling Trench Shape in SiC Power MOSFETs                    | 69 |

### Cover photo:

The demand for power semiconductors, essential devices for reducing energy consumption in order to help curb global warming, has recently been increasing for use as power converters for automobiles (hybrid vehicles) and as power conversion devices for new energy systems such as photovoltaic and wind power generation.

Fuji Electric aims to help protect the global environment by commercializing IGBTs, high performance MOSFETs, power diodes, power ICs and the like, and providing optimal solutions for various fields such as the manufacturing, automotive, information and consumer fields.

The cover photo shows a large capacity (high-power) IGBT module, for which the lineup of the U4-series of 5th generation IGBTs has been expanded. The application of these devices to the high voltage and large capacity inverters used in industrial infrastructure and to the power converters in wind generation systems is expected to increase.

**FUJI ELECTRIC REVIEW vol.55 no.2 2009**

date of issue: May 20, 2009

**editor-in-chief and publisher** Hisao Shigekane  
Technology Strategy Division  
Group Technology and Business Strategy Center  
Fuji Electric Holdings Co., Ltd.  
Gate City Ohsaki, East Tower,  
11-2, Ohsaki 1-chome, Shinagawa-ku,  
Tokyo 141-0032, Japan  
<http://www.fujielectric.co.jp/eng/index.html>

Fuji Electric Holdings Co., Ltd. reserves all rights concerning the republication and publication after translation into other languages of articles appearing herein.

All brand names and product names in this journal might be trademarks or registered trademarks of their respective companies.

**editorial office** Fuji Electric Journal Editorial Office  
c/o Fuji Electric Information Service Co., Ltd.  
9-4, Asahigaoka 1-chome, Hino-shi, Tokyo 191-0065, Japan



# Fuji Electric's Semiconductors: Current Status and Future Outlook

Yasukazu Seki †  
Yoshikazu Takahashi †  
Tatsuhiko Fujihira †

## 1. Introduction

At the July 2008 G8 summit in Toyako Hokkaido, the greatest challenge discussed was global warming. Dire circumstances require recognition of the seriousness of this issue.

In its own business-related activities, Fuji Electric addresses environmental issues by promoting built-in environmental management, aiming “to create efficiency without waste using few natural resources and with low energy consumption” to further advance core technologies cultivated over many years and to make continuous improvements<sup>(1)</sup>.

Power electronics technology, which enables the efficient utilization of electrical power and energy, is positioned a major technology for protecting the global environment and reducing CO<sub>2</sub> emissions. In particular, power semiconductor devices, the key components that support power electronics technology, are expected to become increasingly important.

Environmental friendliness and ease of use are recently being requested of power semiconductors. Of course, components and materials having a deleterious effect on the environment should not be used. In addition to prior requests for lower cost and lower loss, “ease of use” is strongly requested, and technical efforts related to environmental protection, such as efforts to reduce noise, are also included among these requests.

This paper describes the current status and future outlook mainly for Fuji Electric's representative power semiconductor products, power modules, power discretes, power ICs and automotive-use MOSFETs (metal-oxide-semiconductor field-effect transistors).

## 2. Power Modules

Fuji Electric, an industry leader in IGBT (insulated gate bipolar transistor) technology, has begun selling the V-series of 6th generation IGBTs.

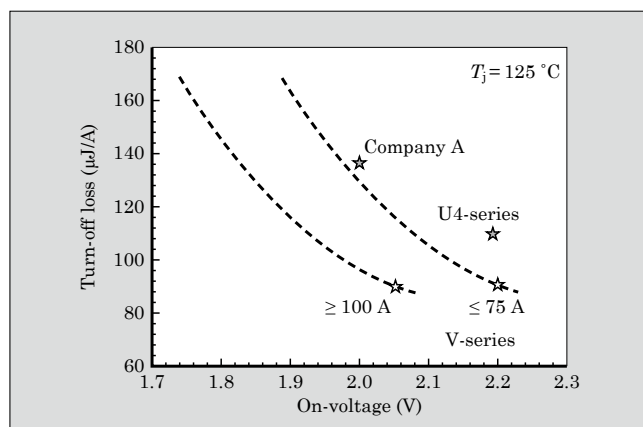
The V-series IGBT modules were designed in consideration of environmental issues, and all packages of this series are RoHS<sup>\*1</sup> compliant. The IGBT

chip structure uses an advanced form of the trench gate structure and field stop structure developed for Fuji Electric's U-series and also realizes lower loss and lower noise. Figure 1 compares the U-series and V-series chip characteristics. The package structure has also been optimized for heat management, and the package size for some current-rated products has been decreased by one rank. Additionally, in response to various customer needs, packages having a solder-free connection structure have also been prepared. Figure 2 shows Fuji Electric's lineup of V-series IGBT module products.

The development of high-power IGBT modules is also accelerating. High-power IGBT modules have begun to be deployed in high-voltage and high-power inverters for power conversion equipment used primarily for industrial infrastructure and in wind power generation systems. As shown in Fig. 3, the high-power modules are equipped with a 5th generation U4-series IGBT chip and are provided as 1,200 V/ 600 to 3,600 A and 1,700 V/ 600 to 3,600 A rated products. These high-power modules use silicon nitride as their substrate material to realize higher current ratings. Ad-

\*1: RoHS is EU directive restricting the use of certain hazardous substances in electrical and electronic equipment.

Fig.1 Comparison of tradeoff for U-series and V-series IGBT chip characteristics



† Fuji Electric Device Technology Co., Ltd.

Fig.2 V-series IGBT module product lineup




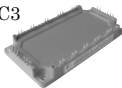
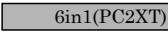

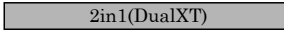





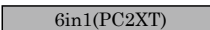

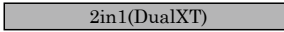

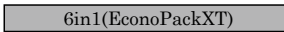
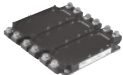

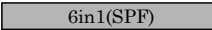

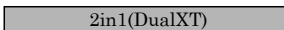
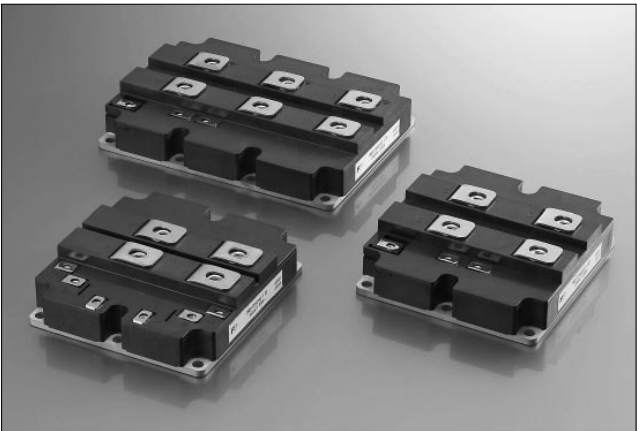
|         |             |        | Main terminal   | 10 (A)  | 15 | 25 | 35 | 50  | 75 | 100 | 150  | 200<br>225   | 300   | 400<br>450  | 600   | 900     | 1,200   |  |
|---------|-------------|--------|---|---------|----|----|----|---|----|-----|--|--|---|---|---|---------|---|--|
| 600 V   | Solder      | Pin    |  | EP2/PC2 |    |    |    |  |    |     |  |  |   | EP3/PC3   |  |         |   |  |
|         |             |        |   |         |    |    |    |  |    |     |  |  |   |   |   |         |   |  |
|         | Screw       |        |   |         |    |    |    |   |    |     | Dual   |  |  |   |   |         |   |  |
|         |             |        |   |         |    |    |    |   |    |     |  |  |   |   |   |         |   |  |
| 1,200 V | Solder      | Pin    |  |         |    |    |    |  |    |     |  |  |   |   |   | EP3/PC3 |   |  |
|         |             |        |   |         |    |    |    |  |    |     |  |  |   |   |   |         |   |  |
|         |             |        |   |         |    |    |    |   |    |     |   |  |   |   |   |         |   |  |
|         |             |        |   |         |    |    |    |   |    |     |  |  |   |   |   |         |   |  |
|         | Screw       |        |   |         |    |    |    |   |    |     | Dual   |  |  |   |   |         |   |  |
|         |             |        |   |         |    |    |    |   |    |     |  |  |  |   |   |         |  |  |
|         | Solder-free | Spring |   |         |    |    |    |  |    |     |  |  |   |   |   |         |   |  |
|         |             |        |   |         |    |    |    |   |    |     |  |  |   |   |   |         |  |  |
|         |             |        |   |         |    |    |    |   |    |     |  |  |   |  |   |         |   |  |

Fig.3 High-power IGBT modules



ditionally, these high-power modules also suppress the generation of noise, and with a 30% reduction in power loss compared to prior products, improved ease of use and enhanced conversion efficiency also contribute to energy savings.

In joint research with Professor Shimada of the Tokyo Institute of Technology, an IGBT module optimized for use in wind power generation was developed using a magnetic energy recovery switch (MERS). The IGBT used in the MERS operates at a switching frequency of several tens of Hz, which is lower than the conventional frequency ( $\leq$  several kHz). On the other hand, because the MERS is connected in series in a power conversion system, increased conduction loss becomes a problem. Thus, upon reconsideration of the tradeoff characteristics, we reduced the on-voltage to 1.54 V to

improve the overall efficiency of the conversion device.

As automotive power module products, a buck-boost converter IGBT IPM (intelligent power module) equipped with a present 5th generation U-series IGBT module and a plated chip mountable on both sides by soldering are being mass-produced and used in the Toyota CROWN\*2 HYBRID, LEXUS\*3 LS600h and LS600hL, and so on.

Next-generation automotive power modules equipped with a 6th V-series IGBT chip and realizing higher power density due to their smaller size and lower power loss can be miniaturized to 40% of the size of prior power module products. Targeting application to mild hybrid systems, next-generation automotive power modules are presently being developed.

IGBT characteristics are already approaching their theoretical limits with the 6th generation V-series IGBTs. For IGBT modules to become even easier to use, improvement in FWD (free wheeling diode<sup>(2)</sup>) characteristics and further package<sup>(3)</sup> research and development are needed. With these comprehensive technologies, IGBT modules can be made to have lower noise, higher reliability and become easier to use.

### 3. Power Discretes

As high-voltage power MOSFETs, Fuji Electric

\*2: CROWN is a registered trademark of Toyota Motor Corporation.

\*3: LEXUS is a registered trademark of Toyota Motor Corporation.

has developed the “SuperFAP-E<sup>3S</sup> low  $Q_g$  series” and the “SuperFAP-E<sup>3</sup> 900 V series.” Recently, in the field of power supply devices that use high-voltage MOSFETs, and particularly as environmental measures, requests for energy savings in various electronic devices have intensified, and at the same time, regulations for higher power efficiency have been strengthened through the International ENERGY STAR program<sup>\*4</sup> standard, and requests for higher efficiency of switching-mode power supplies have also increased. Moreover, in order to satisfy various noise-related regulations, a product must simultaneously satisfy requests both for lower loss and for lower noise. In 2007, Fuji Electric developed and established product lines of its “SuperFAP-E<sup>3</sup> 500 V series” and “SuperFAP-E<sup>3</sup> 600 V series” of 6th generation high-voltage MOSFET products as power MOSFETs for realizing higher efficiency and lower noise in switching-mode power supplies. These product lines feature the industry’s lowest on-resistance for a planar structure. The newly developed SuperFAP-E<sup>3S</sup> low  $Q_g$  series retains the low on-resistance characteristics, gate resistance controllability and low noise performance of the 500 V and 600 V series, while improving the switching performance. The gate charge characteristic  $Q_g$  of the new SuperFAP-E<sup>3</sup> series is lower than that of the prior product series by approximately 20%, and lower switching loss is realized as a result.

Moreover, the SuperFAP-E<sup>3</sup> 900 V series is a higher voltage version of the 500 V and 600 V series. The SuperFAP-E<sup>3</sup> 900 V series suppresses operation in which avalanche current flows into parasitic bipolar transistors and eliminates non-uniform operation among cells during avalanche to realize a damage-resistant device having twice the resistance to avalanche current as the prior product series.

In the high-voltage power MOSFET field, lower cost, smaller size, lower loss and lower noise are strongly requested, and Fuji Electric is focusing on research and development to support these requests.

Looking ahead, research and development is also being advanced to realize both lower resistance and lower cost through the optimal design of super junction MOSFETs<sup>(4)</sup>.

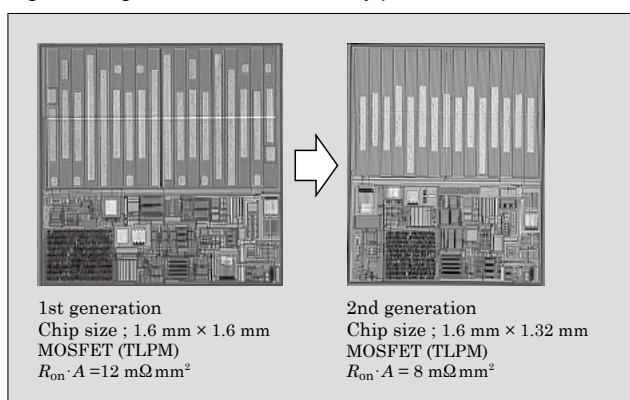
#### 4. Power ICs

The following accomplishments have been realized for power ICs.

- (a) Lithium-ion battery protection IC
- (b) FA5560M combo-IC for critical conduction mode

<sup>\*4</sup>: International ENERGY STAR program is an international environmental labeling system for energy savings in OA equipment, and operates under mutual recognition by the Ministry of Economy, Trade and Industry in Japan and the US Environmental Protection Agency (EPA) in the United States.

Fig.4 2nd generation lithium battery protection IC



PFC current resonance

- (c) Low standby power quasi-resonant power supply controller IC “FA5571 series”
- (d) High efficiency buck converter IC “FA7743N”
- (e) Multi-channel switching DC-DC converter IC “FA7763R” for portable electronic equipment

Practical application of Fuji Electric’s proprietary low on-resistance three-dimensional power device technology enabled lithium-ion battery protection ICs to be mass-produced for the first time in the world. In response to market requests, and as a continuation of the 1st generation products which were mass-produced in 2007, the industry’s highest level of on-resistance of  $R_{on} \cdot A = 8 \text{ m}\Omega \text{ mm}^2$ , where the on-resistance is the resistance per unit area of the power MOSFET, has been achieved. A 2nd generation product has been realized with 17.5% smaller chip size than the 1st generation product. Figure 4 shows photographs of the chips.

To realize lower loss and smaller size in power ICs, the technology for realizing lower loss and smaller size in built-in power devices is critical. Fuji Electric continues to advance research and development for making lower loss and smaller size power devices that are incorporated into power ICs<sup>(5)</sup>.

#### 5. Automotive Devices

- (1) Sophisticated single-chip igniter

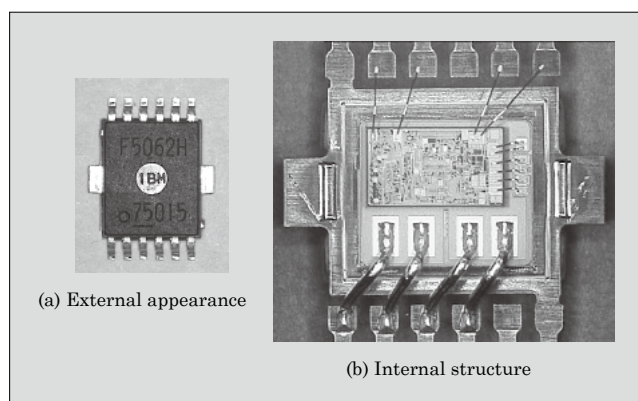
The transition from hybrid type igniters, configured from multiple components, to single-chip igniters is accelerating. In response, a single-chip IGBT incorporating all the relevant protection functions has been commercialized.

The expanded self-protection functionality is a key factor. Functions to prevent damage to the device itself, to prevent the coil from burning, to prevent abnormal ignition from causing engine damage and the like have been realized and the “TO220” single-chip small-size package has been commercialized.

- (2) IPS (intelligent power switch)

Automotive ECUs (engine control units) are installed in an environment that ranges from indoors to the engine compartment, and they are also incorpo-

Fig.5 External appearance and internal structure of COC package



rated into loading equipment and the like, and ECUs are requested to be small in size, have high functionality and be resistance to damage even in harsh environments. Respond to requests for smaller size, Fuji Electric has commercialized product lines of COC (chip on chip) and CSP (chip size package) devices, and also has commercialized a 2-channel product equipped with a status output. No other company provides a 2-channel chip with status output housed in a SOP-8 package.

With newly developed COC technology, the thermal stress behavior of film material for bonding an IC chip in a COC package was analyzed and higher reliability was realized. Figure 5 shows the external appearance and the internal structure of the COC package. As can be seen in the figure, an IC chip is bonded onto a MOSFET chip that has been soldered to the lead frame.

### (3) Pressure sensor

A pressure sensor that uses a CMOS process-based digital trimming scheme has already been introduced to the market as a 5th generation pressure sensor. Applications are primarily for measuring pressure in suction/exhaust systems. Pressure sensors are also actively being developed for new applications, and one such type is the atmospheric pressure sensor, which is used for the purpose of optimizing the engine performance when traveling at a high elevation by providing high elevation compensation for the ECU. Other pressure sensors being developed for new applications

include high-pressure sensors for air conditioners, leakage sensors for fuel tanks, and so on.

Fuji Electric has leveraged the strength of its proprietary technology in response to customer needs for automotive devices. Fuji Electric intends to continue to emphasize cooperation with customers, and to respond to customer needs while aiming to achieve lower prices, smaller size and higher reliability

## 6. Postscript

Under the present circumstances in which environmental issues are beginning to become significant actual problems, corporations have a major role to play. Fuji Electric is moving ahead with efforts to help curb global warming and has positioned these efforts as a vital management task. In the field of power electronics technology, Fuji Electric is working on technical innovations for power semiconductors, the main components in this field, and is endeavoring to make these innovations responsive to the environmental issues.

This paper has described the present status and future outlook for the main products that use power semiconductors. Continuous innovation is needed for all products to achieve lower loss, lower noise, smaller size and higher reliability. Establishing "ease of use" as a product criterion from the customer's prospective, Fuji Electric intends to continue to advance technical development.

## Reference

- (1) Fuji Electric Group Sustainability Report 2008.
- (2) Onozawa, Y. et al. Development of the 1200 V FZ-diode with soft recovery characteristics by the new local lifetime control technique. Proc. of ISPSD '08. p.80.
- (3) Ikeda, Y. et al. A study on the reliability of the chip surface solder joint. Proc. of ISPSD '08. p. 189.
- (4) Sugi, A. et al. Super Junction MOSFETs above 600V with Parallel Gate Structure Fabricated by Deep Trench Etching and Epitaxial Growth. Proc. of ISPSD '08. p. 165.
- (5) Sawada, M. et al. High side n-channel and bidirectional Trench Lateral Power MOSFETs on one chip for DCDC converter ICs. Proc. of ISPSD '08. p. 107.



# IGBT Modules for Hybrid Vehicle Motor Driving

Hiroaki Ichikawa<sup>†</sup>  
Takeshi Ichimura<sup>†</sup>  
Shin Soyano<sup>†</sup>

## 1. Introduction

Influenced by international efforts to curb global warming, automobile manufacturers are focusing on environmental issues and are working to reduce CO<sub>2</sub> emissions. Hybrid vehicles, currently being mass-produced as ecologically friendly cars having low CO<sub>2</sub> emissions, enjoy high public recognition and have rapidly become popular over the past several years.

In a gasoline hybrid system, an electric motor that assists the combustion engine in the range from start-up to low speeds, for which the engine has poor efficiency, and regenerative brakes that efficiently recharge the battery when decelerating are used to improve fuel efficiency.

The main components of a hybrid system are an electric motor, a battery and an inverter. The inverter is used as an electric power conversion system for supplying electrical energy from the battery to the motor, and for storing energy generated by the motor in the battery. IGBT (insulated gate bipolar transistor) modules are generally used as the main switching device in this electric power conversion system.

IGBT modules first began to be used about 20 years ago, primarily in industrial equipment, and are now being used in electric power conversion systems for controlling motors in a wide range of fields, ranging from household appliances such as air conditioners to applications in the railroad industry. In recent years, the range of automotive applications has been expanded and development is aiming to realize IGBT modules having even higher levels of performance.

Hybrid systems can be broadly categorized as either a dual-motor system (traction motor and generation motor) focused on travel performance or a single-motor system that combines traction and generation functions and that is focused on miniaturization. The single-motor hybrid system, known as a parallel hybrid system (hereafter referred to as a parallel hybrid), is expected to increase in popularity with application to small vehicles where the parallel hybrid advantages of small size and light weight can be fully appreciated.

This paper introduces Fuji Electric's automotive IGBT modules that are ideally suited for inverters in parallel hybrids.

## 2. Power Devices for Hybrid Vehicles

To achieve hybridization by installing an inverter, an electric motor and a battery within the limited space of an automobile, the system must be made lighter in weight. To popularize parallel hybrid technology, the capacities of the expensive inverter, motor and battery must be reduced to their respective minimum requirements, and the motors generally used have a capacity of 20 kW or less. To fully utilize the performance advantages of power devices, the rise in device temperature due to the transient maximum current flowing to the motor during acceleration must be limited within an allowable range. Additionally, for the case where the allowable temperature is exceeded, an embedded control that constantly monitors the chip temperature and limits the motor output and a safety design that prevents heat damage to the device due to excessive current must also be provided.

Moreover, the use of electrical regenerative braking (refer to the explanation of regenerative braking on page 50) during deceleration enables energy, which previously was emitted as heat from hydraulic brakes, to be collected as electrical energy and reused in order to improve the fuel economy. The capability to collect as much electric power as possible during the short braking time from the beginning of deceleration until stopping is important, and for this purpose, devices capable of conducting large currents for short time durations are required.

## 3. Characteristics of IGBT Modules for Automobiles

### 3.1 Product specifications

Figure 1 shows the external appearance and Fig. 2 shows an internal block diagram of a Fuji Electric IGBT module. The main characteristics are listed in Table 1, and product features are described below.

(a) 600 V/300 A chip required for inverters that

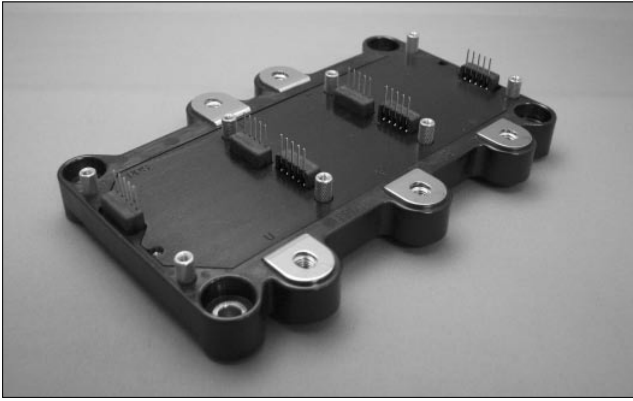
<sup>†</sup> Fuji Electric Device Technology Co., Ltd.



drive 20 kW or smaller 3-phase motors is mounted in a custom 6-in-1 package

- (b) 6th generation 600 V V-series IGBT (realizing a 25% improvement in current density compared to the prior series) is used to realize lower loss and higher current density
- (c) An IGBT with built-in current sensing function and an on-chip temperature sensing diode is used
- (d) Required installation space is reduced through the use of a small and thin module package
- (e) Combination with Fuji Electric's Fi009 gate drive IC enables easy configuration of overheating protection, short-circuit protection and over-current protection functions for the IGBT chip
- (f) Design support is provided by an IGBT module drive evaluation circuit board that facilitates circuit design by the customer

Fig.1 External appearance of IGBT module



- (g) Simultaneous realization of lead-free content and in-vehicle reliability

### 3.2 V-series IGBT chip

The IGBT chip uses Fuji Electric's 6th generation 600 V V-series IGBT chip. A characteristic of this chip is its use of a field-stop (FS) structure and a trench gate, which have a proven track-record with Fuji Electric's 1,200 V IGBTs, to realize a lower collector-emitter saturation voltage. A comparison of output characteristics with conventional products is shown in Fig. 3. For the same chip size, the collector-emitter saturation voltage is reduced by approximately 25% and this new chip is expected to contribute to improved efficiency.

Devices used in automobiles are directly affected by changes in the ambient air temperature and the capability to endure temperature changes (hereafter re-

Fig.2 Internal block diagram

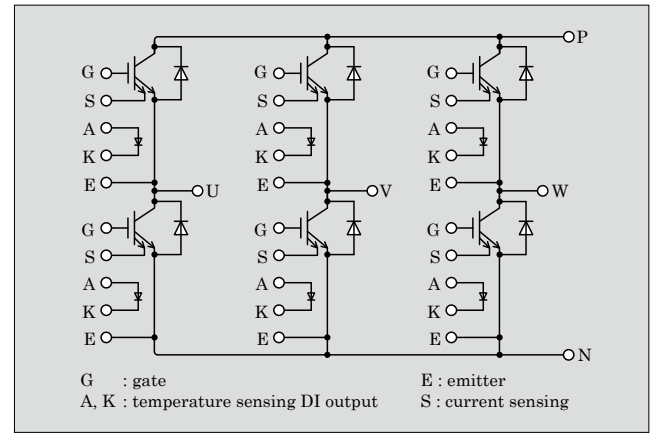


Table 1 Main characteristics

(a) Absolute maximum ratings (unless specified otherwise,  $T_j = T_c = 25^\circ\text{C}$ )

| Item                      | Symbol        | Condition             | Rating          | Unit             |
|---------------------------|---------------|-----------------------|-----------------|------------------|
| Collector-emitter voltage | $V_{CES}$     | $V_{GE} = 0\text{ V}$ | 600             | V                |
| Gate-emitter voltage      | $V_{GES}$     | —                     | $\pm 20$        | V                |
| Collector current         | $I_C$         | Continuous            | 300             | A                |
| Max. allowable loss       | $P_C$         | 1 device              | 595             | W                |
| Max. junction temp.       | $T_{j(\max)}$ |                       | 150             | $^\circ\text{C}$ |
| Operating temp.           | $T_{op}$      |                       | $-30$ to $+125$ |                  |
| Storage temp.             | $T_{stg}$     |                       | $-40$ to $+125$ |                  |

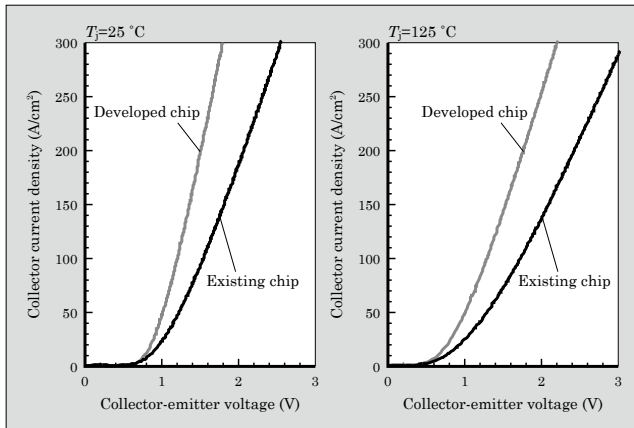
(b) Electrical characteristics (unless specified otherwise,  $T_j = T_c = 25^\circ\text{C}$ )

| Item                                 | Symbol        | Test condition                                     | Min. | Typ. | Max. | Unit |
|--------------------------------------|---------------|--|------|------|------|------|
| Collector cutoff current             | $I_{CES}$     | $V_{GE} = 0\text{ V}$ , $V_{CE} = 600\text{ V}$    | —    | —    | 1.0  | mA   |
| Gate-emitter leakage current         | $I_{GES}$     | $V_{CE} = 0\text{ V}$ , $V_{GE} = \pm 20\text{ V}$ | —    | —    | 200  | nA   |
| Gate-emitter threshold voltage       | $V_{GE(th)}$  | $V_{CE} = 20\text{ V}$ , $I_C = 300\text{ mA}$     | —    | 6.2  | —    | V    |
| Collector-emitter saturation voltage | $V_{CE(sat)}$ | $V_{GE} = 15\text{ V}$ , $I_C = 300\text{ A}$      | —    | 2.10 | 2.63 | V    |
| Forward voltage drop                 | $V_F$         | $I_F = 300\text{ A}$                               | —    | 1.96 | 2.40 | V    |

(c) Thermal characteristics ( $T_c = 25^\circ\text{C}$ )

| Item               | Symbol        | Test condition | Min. | Typ. | Max. | Unit |
|--------------------|---------------|----------------|------|------|------|------|
| Thermal resistance | $R_{th(j-c)}$ | IGBT           | —    | —    | 0.21 | K/W  |
|                    |               | FWD            | —    | —    | 0.25 |      |

Fig.3 Comparison of IGBT output characteristics (comparison with chip characteristics)



ferred to as temperature cycles) is strongly requested. When an IGBT module is exposed to a temperature cycle environment, thermal stress generated at the solder layer in the junction between the insulating substrate and the IGBT chip causes cracks to form and expand. Because the V-series IGBT chip is thinner than the conventional products and deforms flexibly in response to thermal stress, cracks in the solder are less likely to occur even when temperature cycles are added.

### 3.3 Internal temperature during electrical regeneration

During acceleration, a hybrid system requires a large amount of electric power and therefore the battery must always store electrical power. Moreover, during deceleration, the deceleration energy must be converted efficiently into electrical power by electrical regenerative braking. Electrical regenerative braking converts kinetic energy into electric power and charges the battery, and the amount of energy generated is proportional to the mass of the vehicle. In the case where a small motor has been selected, efficiency is increased by regenerating larger amounts of electric power, but the upper limit on the amount of electric power that can be regenerated is constrained by the allowable temperature of a highly conductive FWD chip. Figure 4 shows the internal temperature distribution for the assumed maximum continuous load during electric power regeneration.

By optimizing the chip size and staggering the chip layout in order to improve efficiency during electric power regeneration, the temperatures of the IGBT and FWD chip will be limited to equal values, and the module will simultaneously realize both higher efficiency and smaller size.

### 3.4 On-chip temperature sensing function

If an IGBT is exposed to an environment of anomalous temperature or if the temperature of an IGBT rises suddenly as a result of an abnormal operation, in order to prevent system failure, abnormal heat generation from the IGBT must be sensed and the operation

Fig.4 Internal temperature distribution for assumed regenerative braking

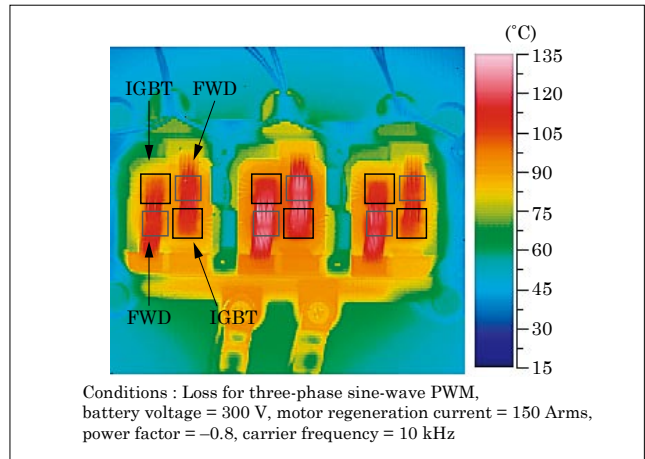
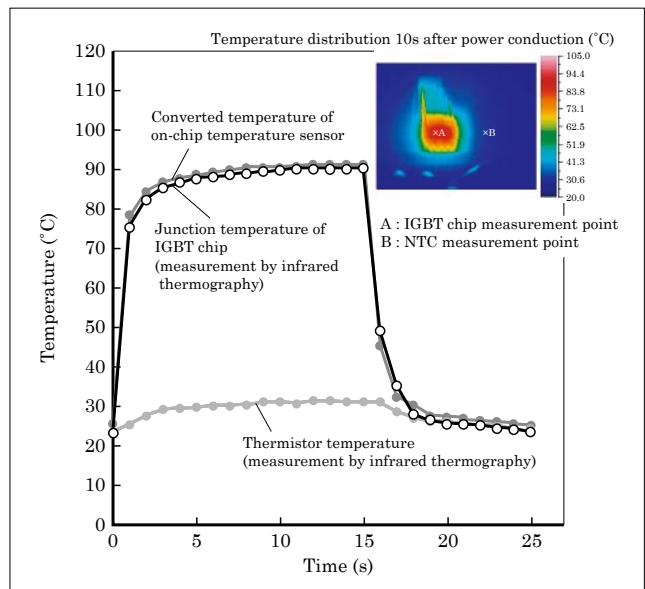


Fig.5 Response characteristics of on-chip temperature sensor



stopped. Hybrid vehicles have a particularly high frequency of motor acceleration and deceleration operations, and therefore are thought to be particularly susceptible to sudden temperature changes resulting from the momentary conduction of electric power. This product is equipped with a diode that is integrated into the IGBT chip as an on-chip temperature sensor. Figure 5 shows the response characteristics of the on-chip temperature sensor.

A comparison of the results of measurement of the IGBT chip surface temperature by infrared thermography with those of the temperature-converted output from the on-chip temperature sensor shows good tracking of temperature changes, even for transient periods on the order of 1 second. Moreover, the capability to compute and sense temperatures even for short durations on the order of 1 ms enables the IGBT to be protected from damage even if a sudden temperature change occurs due to a momentary load fluctuation.

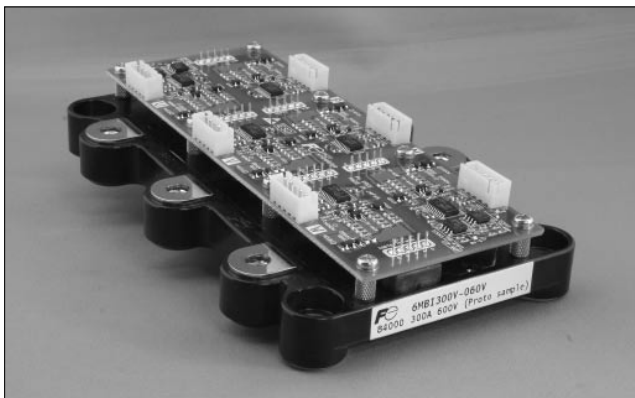
Figure 5 also shows the results of temperature measurement by a NTC (negative temperature coefficient) thermistor that has been mounted near the chip, and a temperature difference of approximately 60 °C from the value sensed by the on-chip temperature sensor can be seen. The reason for this difference is that, in the case where chip temperature rises suddenly in a short time of several tens of seconds or less, heat is radiated primarily from a copper base plate mounted on the bottom surface of the highly thermal-conductive chip package, and the copper base plate has a large thermal time constant in the lateral direction which slows the conduction of heat. However, the protection method of using an NTC thermistor to acquire the transient temperature change of an IGBT chip is limited since the slope of the temperature rise varies according to the value of current flowing into the motor. An on-chip temperature sensor capable of directly sensing the chip temperature is an effective solution for hybrid vehicle-use IGBTs.

#### 4. Drive Circuit Board for Evaluation

To extract the maximum performance from a power device, there must be cooperation between the IGBT drive circuit and protection circuit in the usage environment. Particular care must be taken to avoid incorrect operation due to difficult to discern capacitive coupling and mutual inductions. Moreover, the drive circuit for an IGBT having a built-in on-chip temperature sensor and current sensor which is made from discrete parts, is large in size, and hinders the miniaturization of the inverter and converter unit. In the past, an IGBT IPM (intelligent power module) provided an effective solution to these problems. With a black box-like configuration that makes changes difficult to implement, however, specification changes resulting from an expanded range of applicable vehicle types and the efficient utilization of space by integrating peripheral circuit parts and the printed circuit board were difficult to support.

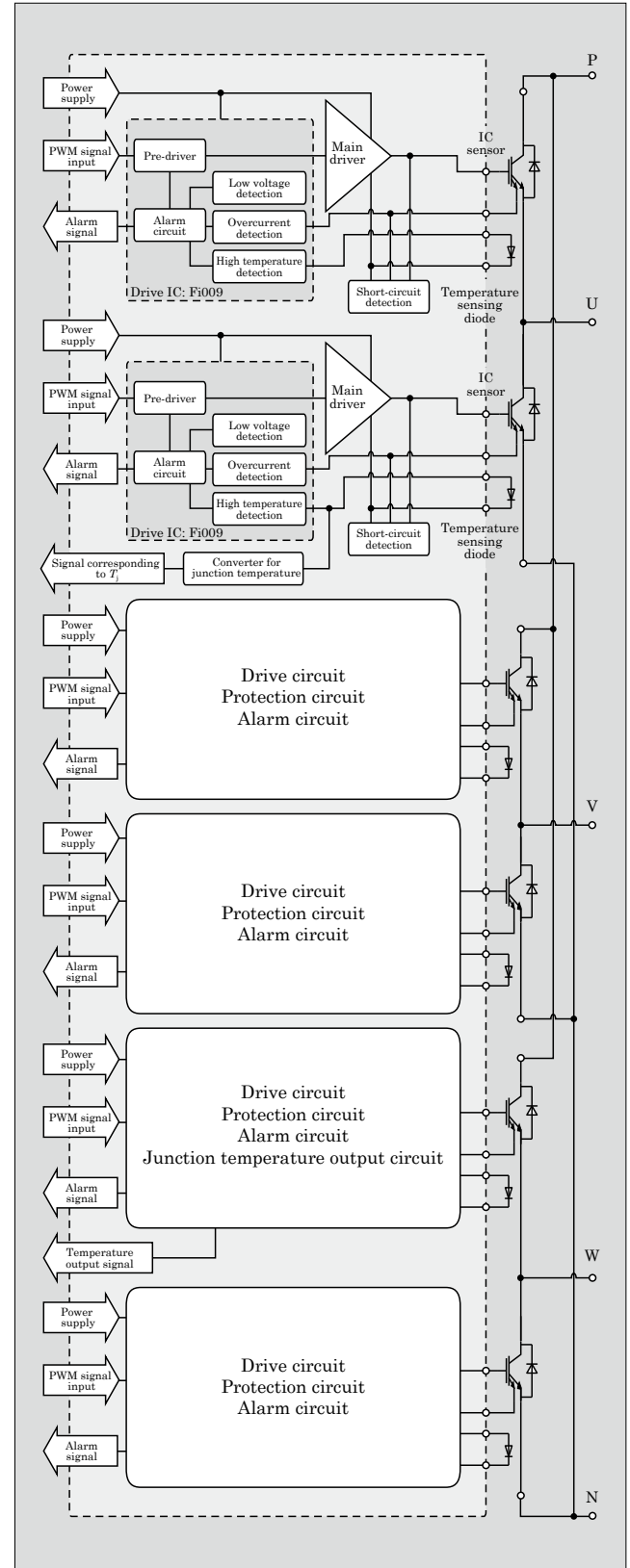
As a solution to the abovementioned problems, we introduce the example of an evaluation drive circuit

Fig.6 Appearance of drive circuit board



board designed especially for the IGBT module. Figure 6 shows the appearance when assembled, and Fig. 7 shows an internal block diagram of the evaluation drive circuit board. By using Fuji Electric's Fi009

Fig.7 Block diagram of evaluation circuit board





IGBT driver IC, which integrates the main drive functions into a single chip, this drive circuit board is configured with a fewer number of parts. The drive circuit board is extremely versatile and is also configured with discrete parts at locations where changes in the time constant are envisioned due to changes in the IGBT module specifications and in the customer usage environment. Moreover, to protect the IGBT, short-circuit protection, overcurrent protection, and overheating protection using an IGBT on-chip temperature sensor are provided, and the board is designed so that the IGBT operation can be stopped safely if necessary. A circuit for externally outputting the temperature being monitored by the on-chip temperature sensor is provided on each of the upper and lower arms. These output circuits enable observation of the IGBT chip

temperature during evaluation.

## 5. Postscript

This paper has introduced Fuji Electric's automotive IGBT modules for use in parallel hybrid vehicles. The integration of 6th generation IGBTs into custom packages for automobile use is expected to contribute to the realization of even smaller size and higher performance inverter units.

Fuji Electric intends to continue its efforts toward achieving higher performance and higher reliability elements, and to help protect the global environment by reducing CO<sub>2</sub> emissions and increasing the fuel efficiency of hybrid vehicles.



### **Explanation** Regenerative braking

Regenerative braking uses the motor as an electric generator to convert kinetic energy, emitted during deceleration as heat by hydraulic brakes, into electric power and to charge the battery. Because regenerative brakes are non-contact and

do not involve mechanical friction, a regenerative braking system is highly effective in reducing energy consumption and enables electric power to be reused without generating heat.

# High-power IGBT Modules

Takashi Nishimura †  
Yoshikazu Takamiya †  
Osamu Nakajima †

## 1. Introduction

To help curb global warming, clean energy, rather than fossil fuels, has been used increasingly in recent years. Markets for new types of energy (wind-power generation, solar-power generation) capable of supplying electric power without emitting green house gases (CO<sub>2</sub>) are growing rapidly, and the inverter systems used in these fields are trending toward higher power capacities.

The main power device in industrial-use high-power inverter systems is the GTO (gate turn-off) thyristor, which easily handles high voltages and currents. However, as a result of outstanding advances in technologies for increasing the voltage and power capacities of IGBT (insulated gate bipolar transistor) modules, GTO thyristors in high-voltage and high-power applications are being replaced by IGBT modules which have an insulated structure that facilitates assembly, handling and maintenance inspections. Fuji Electric has expanded its IGBT product lineup by developing

high-power IGBT modules for industrial, high-power applications.

Targeting applications in the growing field of new energy, Fuji Electric has newly developed 1,200 V and 1,700 V high-power IGBT modules equipped with U4 chips, an improved version of the U-series chips, and that feature enhanced thermal characteristics and significantly improved environmental durability. This paper presents an overview and discusses the technical development of the modules.

## 2. Product Lineup

Table 1 shows Fuji Electric's product lineup of newly developed high-power IGBT modules. A 1-in-1 package has a current capacity of 1,200 to 3,600 A and a 2-in-1 package has a current capacity of 600 to 1,200 A, and the module voltages are 1,200 V or 1,700 V for a total of 14 models. Figure 1 shows an external view of the packages.

Table 1 Fuji Electric's product lineup of high-power IGBT modules

|        | Package type | Package size (mm) | CTI*        | Insulating substrate                              | Base        | Rated voltage (V) | Rated current (A) | Model number    |
|--------|--------------|-------------------|-------------|---|-------------|-------------------|-------------------|-----------------|
| 1 in 1 | M151         | 130 × 140 × 38    | 600 or more | Silicon nitride (Si <sub>3</sub> N <sub>4</sub> ) | Copper (Cu) | 1,200             | 1,200             | 1MBI1200U4C-120 |
|        |              |                   |             |   |             |                   | 1,600             | 1MBI1600U4C-120 |
|        |              |                   |             |   |             | 1,700             | 1,200             | 1MBI1200U4C-170 |
|        |              |                   |             |   |             |                   | 1,600             | 1MBI1600U4C-170 |
|        | M152         | 190 × 140 × 38    |             |   |             | 1,200             | 2,400             | 1MBI2400U4D-120 |
|        |              |                   |             |   |             |                   | 3,600             | 1MBI3600U4D-120 |
|        |              |                   |             |   |             | 1,700             | 2,400             | 1MBI2400U4D-170 |
|        |              |                   |             |   |             |                   | 3,600             | 1MBI3600U4D-170 |
| 2 in 1 | M256         | 130 × 140 × 38    | 600 or more | Silicon nitride (Si <sub>3</sub> N <sub>4</sub> ) | Copper (Cu) | 1,200             | 600               | 2MBI600U4G-120  |
|        |              |                   |             |   |             |                   | 800               | 2MBI800U4G-120  |
|        |              |                   |             |   |             |                   | 1,200             | 2MBI1200U4G-120 |
|        |              |                   |             |   |             | 1,700             | 600               | 2MBI600U4G-170  |
|        |              |                   |             |   |             |                   | 800               | 2MBI800U4G-170  |
|        |              |                   |             |   |             |                   | 1,200             | 2MBI1200U4G-170 |

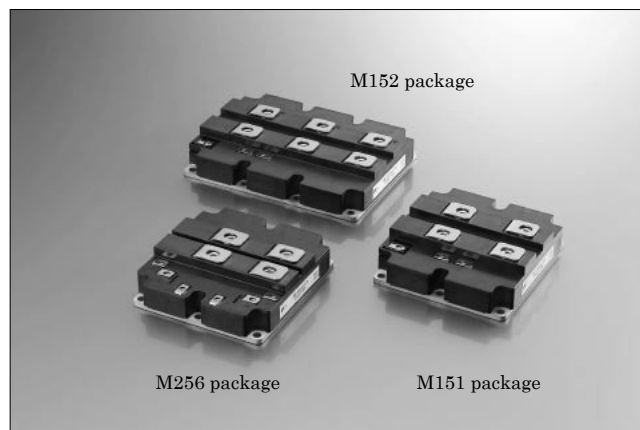
\*CTI : Comparative Tracking Index

† Fuji Electric Device Technology Co., Ltd.

### 3. Electrical Characteristics

Electrical characteristics of the 2MBI800U4G-170 (2-in-1, 800 A/1,700 V), a representative model, are described below. The maximum rated values and characteristics are listed in Table 2.

Fig.1 External view of Fuji Electric's high-power IGBT modules



#### 3.1 V-I characteristics

By reducing the injection efficiency of the pnp transistor, increasing the transport efficiency without using lifetime control, and providing a positive temperature coefficient, the collector-emitter saturation voltage characteristic of the IGBT chip has been improved to achieve higher performance. Also, in the FWD (free wheeling diode) chip, carrier lifetime control was optimized so the forward voltage has a positive temperature coefficient as in the IGBT.

When the junction temperature increases, a chip having a positive temperature coefficient acts to equalize the junction temperature among chips connected in parallel and performs self-balancing to balance the current, and is therefore suitable for use with configurations in which many chips are connected in parallel for high-power IGBT modules. Figure 2 shows the collector-emitter saturation voltage vs. collector current characteristics and Fig. 3 shows the forward voltage vs. forward current characteristics.

Table 2 Absolute maximum ratings and characteristics (Model: 2MBI800U4G-170)

(a) Maximum ratings ( $T_j = T_c = 25^\circ\text{C}$ , unless otherwise indicated)

| Item                       | Symbol         | Condition             |                          | Rating      | Unit             |
|----------------------------|----------------|-----------------------|--------------------------|-------------|------------------|
| Collector-emitter voltage  | $V_{CES}$      | $V_{GE} = 0\text{ V}$ |                          | 1,700       | V                |
| Gate-emitter voltage       | $V_{GES}$      | —                     |                          | $\pm 20$    | V                |
| Collector current          | $I_{C(DC)}$    | Continuous            | $T_c = 80^\circ\text{C}$ | 800         | A                |
|                            | $I_{C(pulse)}$ | 1 ms                  | $T_c = 80^\circ\text{C}$ | 1,600       | A                |
| Max. collector dissipation | $P_C$          | 1 device              |                          | 4,800       | W                |
| Max. junction temperature  | $T_{jmax}$     | —                     |                          | 150         | $^\circ\text{C}$ |
| Storage temperature        | $T_{stg}$      | —                     |                          | -40 to +125 | $^\circ\text{C}$ |
| Isolation voltage          | $V_{iso}$      | AC : 1 minute         |                          | 3,400       | V                |

(b) Electrical characteristics ( $T_j = T_c = 25^\circ\text{C}$ , unless otherwise indicated)

| Item  | Symbol        | Condition   | Min.                      | Typical | Max. | Unit          |
|---|---------------|---|---------------------------|---------|------|---------------|
| Collector-emitter leakage current           | $I_{CES}$     | $V_{GE} = 0\text{ V}$ , $T_j = 125^\circ\text{C}$ , $V_{CE} = 1,700\text{ V}$                             | —                         | —       | 1.0  | mA            |
| Gate-emitter leakage current                | $I_{GES}$     | $V_{GE} = \pm 20\text{ V}$  | —                         | —       | 2.4  | $\mu\text{A}$ |
| Gate-emitter threshold voltage              | $V_{GE(th)}$  | $V_{CE} = 20\text{ V}$ , $I_C = 0.8\text{ A}$   | 5.5                       | 6.5     | 7.5  | V             |
| Collector-emitter saturation voltage (chip) | $V_{CE(sat)}$ | $V_{GE} = +15\text{ V}$ ,<br>$I_C = 800\text{ A}$   | $T_j = 25^\circ\text{C}$  | 2.25    | 2.40 | V             |
|   |               |   | $T_j = 125^\circ\text{C}$ | 2.65    | —    |               |
| Input capacitance                           | $C_{ies}$     | $V_{GE} = 0\text{ V}$ , $V_{CE} = 10\text{ V}$ , $f = 1\text{ MHz}$                                       | —                         | 75      | —    | nF            |
| Turn-on time                                | $t_{on}$      | $V_{CC} = 900\text{ V}$ , $I_C = 800\text{ A}$<br>$V_{GE} = \pm 15\text{ V}$<br>$T_j = 125^\circ\text{C}$ | —                         | 3.10    | —    | $\mu\text{s}$ |
|   | $t_r$         |   | —                         | 1.25    | —    |               |
| Turn-off time                               | $t_{off}$     |   | —                         | 1.45    | —    |               |
|   | $t_f$         |   | —                         | 0.25    | —    |               |
| Forward voltage (chip)                      | $V_f$         | $V_{GE} = 0\text{ V}$ ,<br>$I_f = 800\text{ A}$   | $T_j = 25^\circ\text{C}$  | 1.80    | 2.15 | V             |
|   |               |   | $T_j = 125^\circ\text{C}$ | 2.00    | —    |               |
| Reverse recovery time                       | $t_{rr}$      | $V_{CC} = 900\text{ V}$ , $I_F = 800\text{ A}$ , $T_j = 125^\circ\text{C}$                                | —                         | 0.45    | —    | $\mu\text{s}$ |

(c) Thermal characteristics

| Item                          | Symbol        | Condition | Min. | Typical | Max.  | Unit |
|-------------------------------|---------------|-----------|------|---------|-------|------|
| Thermal resistance (1 device) | $R_{th(j-C)}$ | IGBT      | —    | —       | 0.026 | K/W  |
|                               |               | FWD       | —    | —       | 0.045 |      |



### 3.2 Switching characteristics

Optimization of the balance between input capacitance ( $C_{ies}$ ) and reverse transfer capacitance ( $C_{res}$ ) in a U4-series IGBT chip provides the chip with such characteristics as significantly lower turn-on loss, reduced  $di/dt$  during low current, improved controllability of turn-on  $di/dt$  by gate resistance, and reduced surge voltage during reverse recovery. Figure 4 shows turn-on, turn-off and reverse recovery waveforms for a module at the rated current (800 A) under the conditions of  $V_{CC}=900$  V,  $R_{g(on)}=4.7\ \Omega$ ,  $R_{g(off)}=1.2\ \Omega$  and  $T_j=125\ ^\circ\text{C}$ . The switching loss was 257 mJ during turn-on, 254 mJ during turn-off, and 228 mJ during reverse recovery. Figure 5 shows the current dependency of the switching loss and Fig. 6 shows the gate resistance dependency of the switching loss.

Fig.2 Output characteristics

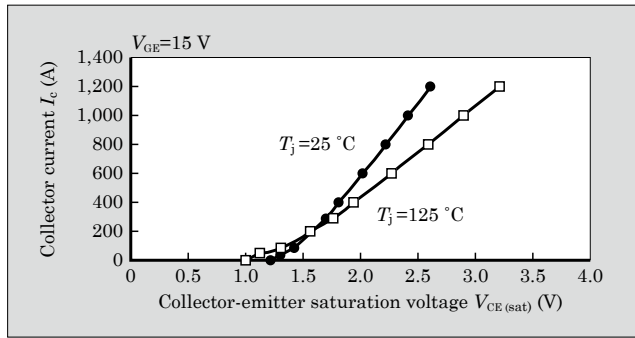


Fig.3 Forward  $I$ - $V$  characteristics

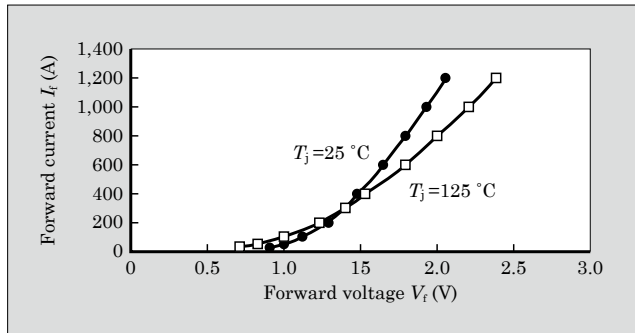
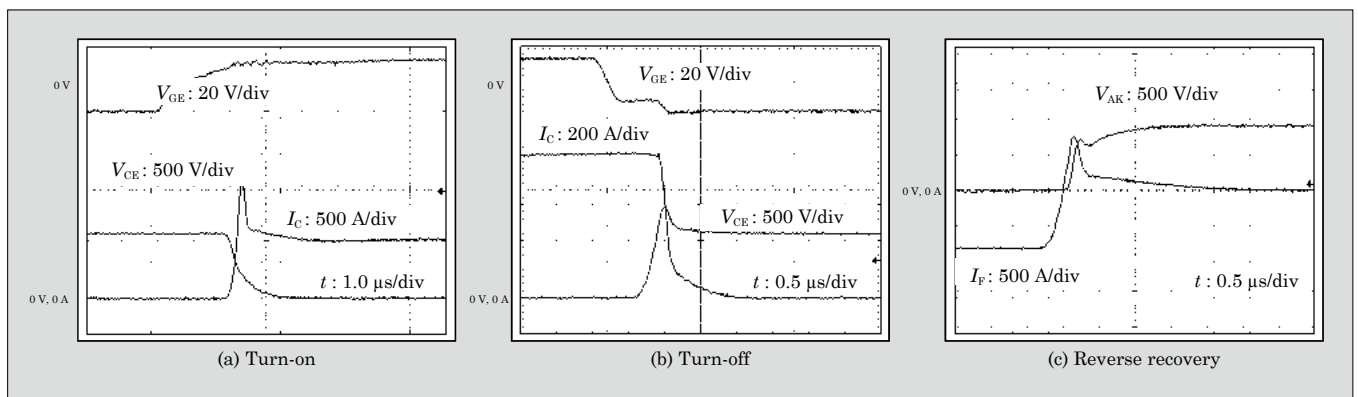


Fig.4 Switching waveforms (inductive load)



## 4. Package Technologies

### 4.1 Reduction in thermal resistance

The majority of industrial-use high-power inverter systems achieve greater power by connecting many modules in a serial and parallel configuration. Customer needs for system downsizing result in higher densities. Reducing the size of cooling fins that radiate heat generated by the module results in decreased heat dissipation efficiency and leads to higher junction temperatures in the semiconductor chip. Higher junction temperatures raise concern about the reliability of a module, and therefore junction temperatures must be reduced. The following three methods can be used for this purpose.

Fig.5 Switching loss dependency on  $I_c$ ,  $I_f$

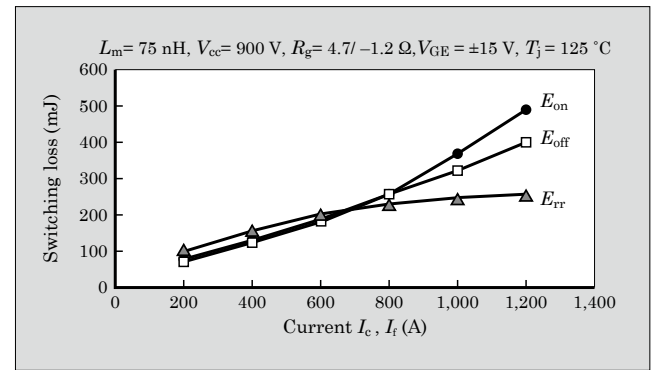
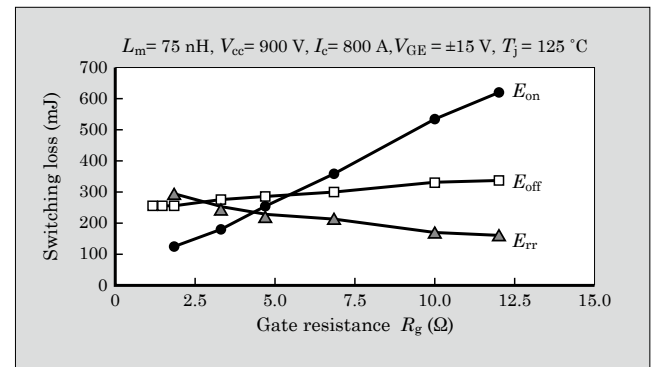


Fig.6 Switching loss dependency on  $R_g$



- Reduce the amount of heat generated by the module
- Reduce the thermal resistance (between the junction area and case) of the module
- Improve the heat dissipation efficiency of the cooling fins

Two of the above methods can be implemented with a module itself: reducing the amount of generated heat and reducing the thermal resistance. The ability to reducing the amount of generated heat largely depends on the chip characteristics, and next-generation chip technology is eagerly awaited. On the other hand, a reduction in thermal resistance can be achieved, regardless of the chip characteristics, by optimizing the module structure.

Figure 7 shows the results of a thermal simulation of a conventional high-power IGBT module that uses a DCB (direct copper bonding) substrate made of aluminum oxide ( $\text{Al}_2\text{O}_3$ ). Since the thermal resistance of the DCB substrate accounts for approximately 52% of

Fig.7 Thermal resistance of each layer (by percentage)

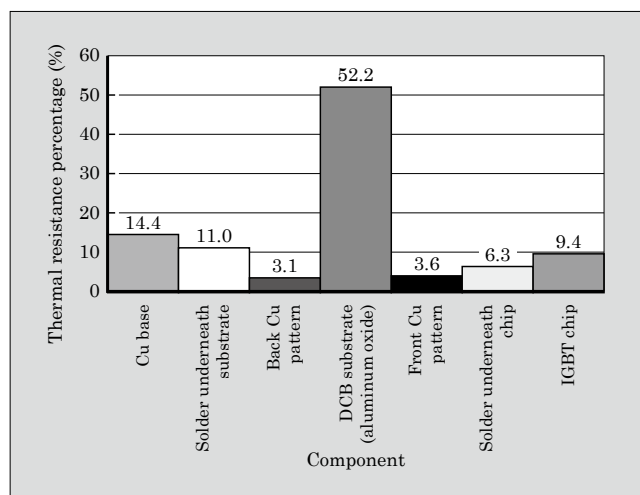


Table 3 Comparison of various DCB substrates

|                                     | Aluminum oxide<br>$\text{Al}_2\text{O}_3$ | Aluminum oxide<br>$\text{Al}_2\text{O}_3$ | Silicon nitride<br>$\text{Si}_3\text{N}_4$ | Aluminum nitride<br>$\text{AlN}$         |
|-------------------------------------|---|---|--|--|
| Thickness                           | 0.32 mm                                   | 0.32 mm                                   | 0.32 mm                                    | 0.65 mm                                  |
| Heat transfer coefficient           | × (21 $\text{W}/(\text{m}^2\text{K})$ )   | △ (24 $\text{W}/(\text{m}^2\text{K})$ )   | ○ (90 $\text{W}/(\text{m}^2\text{K})$ )    | ◎ (170 $\text{W}/(\text{m}^2\text{K})$ ) |
| Bending strength                    | ○   | △   | ◎  | ×  |
| Insulation breakdown voltage        | ◎   | ◎   | ◎  | ◎  |
| Cost                                | ◎   | △   | △  | ×  |
| Easy of assembly                    | ○   | ○   | △  | △  |
| Thermal resistance reduction effect | ×   | △   | ○  | ◎  |

◎ : Excellent ○ : Good △ : Fair × : Poor

the thermal resistance of the entire module, we determined that reducing the thermal resistance of the DCB substrate would be the most effective way to reduce the total thermal resistance. Table 3 lists the results of comparison of various DCB substrates, and Fig. 8 shows the results of comparison by thermal simulation of module thermal resistance. In selecting a DCB substrate, we took a comprehensive approach that considered such factors as the thermal resistance reduction effect, ease of assembly, cost and so on, and decided to use silicon nitride ( $\text{Si}_3\text{N}_4$ ) for which a significant thermal resistance reduction effect can be expected. We measured the thermal resistance and verified reductions in thermal resistance of 33% at the IGBT area and 31% at the FWD area as compared to the case of the aluminum oxide substrate.

## 4.2 Improved environmental characteristics of molded package

When a molded package is placed under a strong electric field, dust and moisture adhering to the surface of the molded package carbonize and form carbonized tracks, which may lead to decreased insulation and sometimes to insulation breakdown. In some cases there is a risk of fire. Wind-power and solar-power generators are often installed at sites having high grit, dust and salinity content, and high humidity. For high-power IGBT modules to be usable in such an environment, the development of a molded package that is resistant to the formation of carbonized tracks is essential. The following two methods exist for realizing molded packages that are resistant to the formation of carbonized tracks.

- Lengthen the creepage surface (carbonized track) of the molded package
- Use mold resin that resists forming carbonized tracks

To lengthen the creepage surface of the molded

Fig.8 Comparison by thermal simulation of module thermal resistance

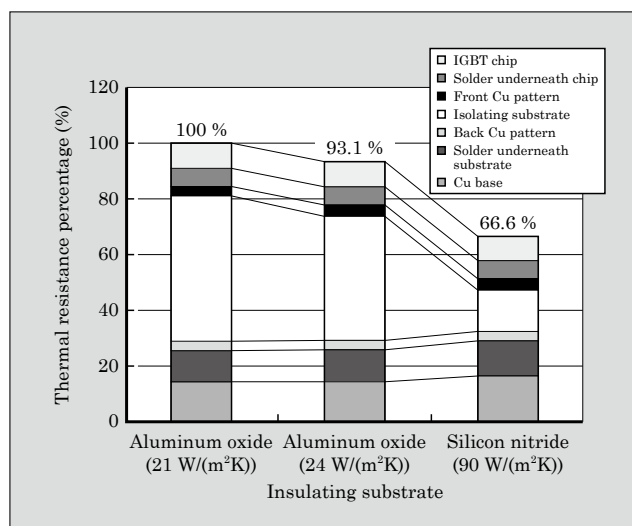


Table 4 Comparative tracking index

|                                   | PLC * | CTI : Comparative tracking index |
|-----------------------------------|-------|----------------------------------|
| High level<br>↑<br>↓<br>Low level | 0     | $600 \leq \text{CTI}$            |
|                                   | 1     | $400 \leq \text{CTI} < 600$      |
|                                   | 2     | $250 \leq \text{CTI} < 400$      |
|                                   | 3     | $175 \leq \text{CTI} < 250$      |
|                                   | 4     | $100 \leq \text{CTI} < 175$      |
|                                   | 5     | $\text{CTI} < 100$               |

\* PLC : Performance Level Category

package, the surface of the molded package must have uneven shape, and in order to prevent an increase in external dimensions that would forfeit compatibility with competitors' package sizes, Fuji Electric selects and uses a mold resin having a CTI (comparative tracking index) of one rank higher. Table 4 shows the tracking index ranges. The highest level is assigned to the tracking index range of  $600 \leq \text{CTI}$ .

## 5. Power Cycle Capability

Inheriting the same high-power package technology as the conventional high-power IGBT module, this newly developed high-power IGBT module uses high-rigidity Sn-Ag solder for soldering underneath the chip, partitions the DCB substrate into several segments to suppress thermal interference among the

DCB substrates, and has a main terminal structure that equalizes current among the DCB substrates. Additionally, by optimizing the thickness of the solder underneath the DCB substrate and by improving the method of production, the  $\Delta T_j$  power cycle was confirmed to be equivalent to that of a conventional module having a smaller number of chips connected in a parallel configuration. Furthermore, in a  $\Delta T_c$  power cycle test where the package temperature changes significantly for a characteristic high-power IGBT module application, 10,000 cycles were verified at the condition of  $\Delta T_c = 70^\circ\text{C}$

## 6. Postscript

This paper has introduced Fuji Electric's improved high-power IGBT module products, which are equipped with a U4-series chip and that feature enhanced thermal characteristics and improved environmental durability. These modules constitute a product group capable of meticulous supporting not only the diversifying needs of the high-power field, but also the needs of the rapidly growing field of new energy.

To support these increasing needs, Fuji Electric intends to continue to advance power semiconductor and package technologies, and to develop new products that contribute to the progress of power electronics.





# 6th Generation Power MOSFET Super FAP-E<sup>3S</sup> Low Q<sub>g</sub> Series

Ryu Araki<sup>†</sup>  
Yukihito Hara<sup>†</sup>  
Sota Watanabe<sup>†</sup>

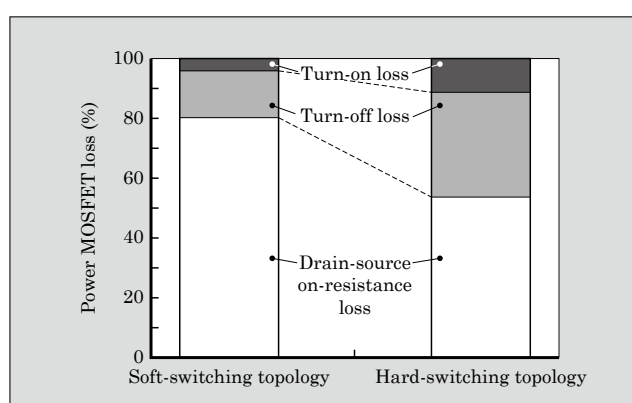
## 1. Introduction

In recent years, efforts to address environmental issues have focused on the goal of reducing greenhouse effect gases, while at the same time, in consideration of future energy supply and demand trends associated with the economic growth of developing nations such as the ASEAN and BRICs countries, the trend toward energy savings is accelerating. In particular, energy savings is demanded in various electronic devices that have rapidly come into widespread use, and as a result of the International ENERGY STAR program\*<sup>1</sup>, power efficiency improvements are regulated, and requests for higher efficiency are intensifying for the switched-mode power supplies that supply electric power to such electronic devices. Requests for lower noise to comply with various noise regulations must also be supported.

Consequently, the power devices installed in switched-mode power supplies that support these requests are required to have low loss and low noise. The power devices are also required to be resistant to damage and easy to use.

Various converter topologies have been proposed for switching-mode power supplies, and soft-switching topologies such as a current resonant type converter, a quasi-resonant converter and the like have been used increasingly in the main converter unit, but many hard-switching topologies are used in the conventional flyback topology, forward topology and power factor improvement circuits (PFC: power factor correction). Figure 1 shows results of the loss analysis of a power MOSFET (metal-oxide-semiconductor field-effect transistor) for both soft-switching and hard-switching topologies. With a soft-switching topology, the drain-source on-resistance loss becomes predominant and therefore devices having low on-resistance characteristics are demanded. On the other hand, with a hard-switching topology, the drain-source on-resistance loss and the turn-off loss account for the majority of loss, and therefore power devices suitable for this circuit are requested to have lower on-resistance, and to improve of switching performance.

Fig.1 Power MOSFET loss analysis results for soft-switching and hard-switching topologies



Fuji Electric's "SuperFAP-E<sup>3</sup> series" general-purpose product lineup exhibits the characteristics of both low loss as a result of low on-resistance and low noise, and is already an established series of power MOSFETs for realizing higher efficiency and lower noise in switched mode power supplies.

The "SuperFAP-E<sup>3S</sup> low Q<sub>g</sub> series" of 6th generation power MOSFETs retains the low on-resistance, low noise performance and gate resistance controllability of the prior product series while providing improved switching performance, and was developed for PWM (pulse width modulation)-ICs (hard-switching topology). Characteristics and applied results of this new series are described below.

## 2. Product Overview

The newly developed SuperFAP-E<sup>3S</sup> low Q<sub>g</sub> series for PWM-ICs (hard-switching topology) retains the on-resistance performance, i.e., the industry's lowest on-resistance for a planar type MOSFET, of the existing

<sup>†</sup> Fuji Electric Device Technology Co., Ltd.

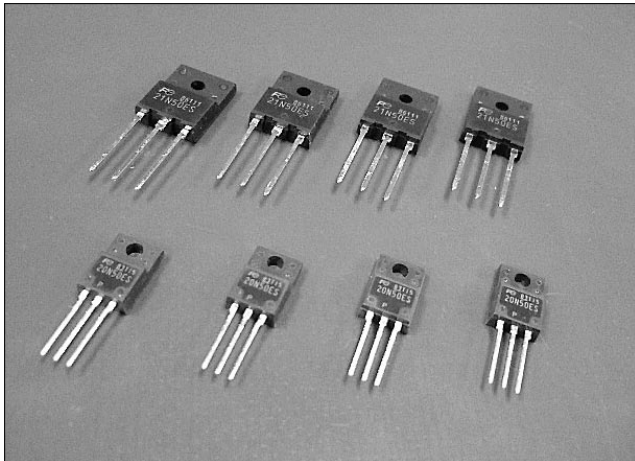
\*1: International ENERGY STAR program is an international environmental labeling system for energy savings in OA equipment, and operates under mutual recognition by the Ministry of Economy, Trade and Industry in Japan and the US Environmental Protection Agency (EPA) in the United States.

SuperFAP-E<sup>3</sup> series while realizing an approximate 20% reduction in gate charge  $Q_g$  compared to the previous series and lower switching loss. Table 1 compares representative electrical characteristics of the new products with those of the prior product series. Figure 2 shows the appearance of the new products and Table 2 lists the products in the 500 V and 600 V series. Specific design measures are described below.

Table 1 Comparison of characteristics

|                 | SuperFAP-E <sup>3S</sup><br>low $Q_g$ series | SuperFAP-E <sup>3</sup> series<br>(prior product) |
|-----------------|--|---|
| Model           | FMV23N50ES                                   | FMV23N50E   |
| Package         | TO-220F                                      | TO-220F   |
| $V_{DS}$        | 500 V  | 500 V   |
| $I_D$           | 23 A   | 23 A  |
| $R_{DS(on)max}$ | 0.245 $\Omega$                               | 0.245 $\Omega$                                    |
| $V_{GS}$        | 4.2 V (typ.)                                 | 3 V (typ.)  |
| $g_{fs}$        | 16 S (typ.)                                  | 28 S (typ.)                                       |
| $Q_G$           | 76 nC (typ.)                                 | 93 nC (typ.)                                      |

Fig.2 Appearance of new products



### 3. Applied Technology

The SuperFAP-E<sup>3S</sup> low  $Q_g$  product is based on the SuperFAP-E<sup>3</sup> concept of “low loss due to low on-resistance characteristics, low noise, and being resistant to damage and easy to use” and additionally aims to improve the switching characteristics.

The  $Q_g$  was lowered in order to reduce the turn-off loss and to improve the switching performance. Further, the gain characteristic,  $g_{fs}$ , was reduced in order to reduce noise caused by the rush current at turn-on.

As a measure for reducing  $Q_g$  and  $g_{fs}$ , we increased the thickness of the gate oxide layer. Increasing the thickness of the gate oxide layer causes the gate threshold voltage  $V_{GS(th)}$  to rise and the on-resistance to increase, and therefore, improved switching performance and lower on-resistance characteristics are difficult to realize simultaneously. The film thickness must be increased within the range that does not degrade the on-resistance. Considering that the driving voltage of a PWM-IC for a typical switching-mode power supply is at least 10 V, the film thickness was increased by approximately 30% compared to the prior product series. Moreover, if the thickness of the gate oxide film is increased, the diffusion shape will change, maintaining the QPJ (quasi-plane-junction) structure at the same level as with the SuperFAP-E<sup>3</sup> series will become difficult, and the breakdown voltage will decrease. Accordingly, the concentrations of the surface n layer and the channel p diffusion layer are optimized to ensure the same breakdown voltage as with the prior product series.

As shown in Fig. 3, the aforementioned design enables the gate charge  $Q_g$  to be reduced by approximately 20% compared to the prior product series. Additionally, by maintaining the QPJ structure, reducing the channel density and optimizing the surface structure, the  $g_{fs}$  gain characteristic is reduced by approximately 40% compared to the prior product series, as shown in Fig. 4.

Table 2 SuperFAP-E<sup>3S</sup> low  $Q_g$  series product list

| Breakdown voltage<br>$BV_{DSS}$ | Rated current<br>$I_D$ | On-resistance<br>$R_{DS(on)}$ | Gate charge<br>$Q_g$ | Package    |            |            |            |            |
|---------------------------------|------------------------|-------------------------------|----------------------|------------|------------|------------|------------|------------|
|                                 |                        |                               |                      | TO-220     | TO-220F    | T-pack     | TO-3P      | TO-3PF     |
| 500 V                           | 12 A                   | 0.52 $\Omega$                 | 36 nC                | FMP12N50ES | FMV12N50ES | FMI12N50ES | —          | —          |
|                                 | 16 A                   | 0.38 $\Omega$                 | 48 nC                | FMP16N50ES | FMV16N50ES | FMI16N50ES | FMH16N50ES | —          |
|                                 | 20 A                   | 0.31 $\Omega$                 | 59 nC                | FMP20N50ES | FMV20N50ES | FMI20N50ES | —          | —          |
|                                 | 21 A                   | 0.27 $\Omega$                 | 66 nC                | —          | FMV21N50ES | —          | FMH21N50ES | FMR21N50ES |
|                                 | 23 A                   | 0.245 $\Omega$                | 72 nC                | —          | FMV23N50ES | —          | FMH23N50ES | FMR23N50ES |
|                                 | 28 A                   | 0.19 $\Omega$                 | 100 nC               | —          | FMV28N50ES | —          | FMH28N50ES | FMR28N50ES |
| 600 V                           | 6 A                    | 1.2 $\Omega$                  | 27 nC                | FMP06N60ES | FMV06N60ES | FMI06N60ES | —          | —          |
|                                 | 12 A                   | 0.75 $\Omega$                 | 37 nC                | FMP12N60ES | FMV12N60ES | FMI12N60ES | —          | —          |
|                                 | 16 A                   | 0.47 $\Omega$                 | 58 nC                | FMP16N60ES | FMV16N60ES | FMI16N60ES | —          | —          |
|                                 | 17 A                   | 0.40 $\Omega$                 | 69 nC                | —          | FMV17N60ES | —          | FMH17N60ES | FMR17N60ES |
|                                 | 19 A                   | 0.365 $\Omega$                | 81 nC                | —          | FMV19N60ES | —          | FMH19N60ES | FMR19N60ES |
|                                 | 23 A                   | 0.28 $\Omega$                 | 100 nC               | —          | —          | —          | FMH23N60ES | FMR23N60ES |

Fig.3  $Q_g$  comparison

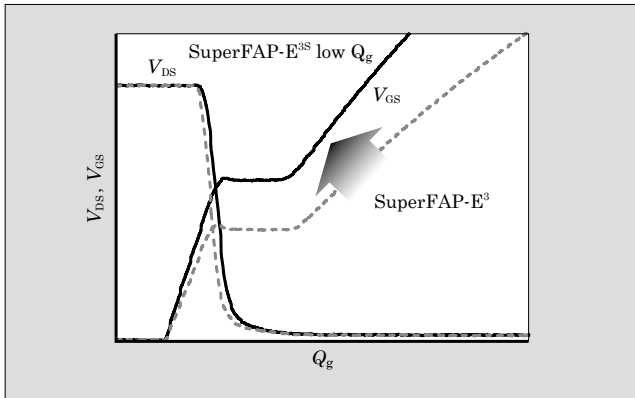


Fig.4  $g_{fs}$  comparison

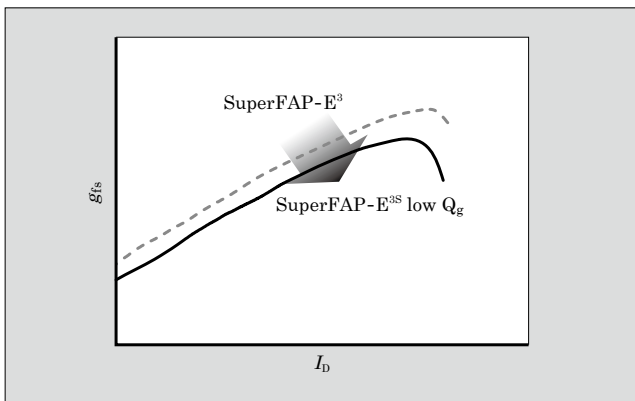
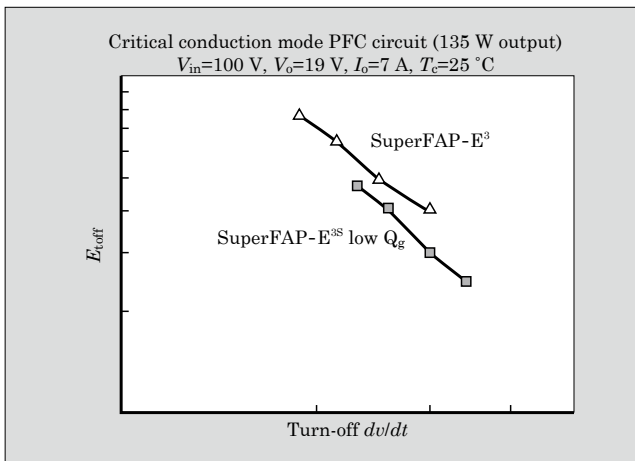


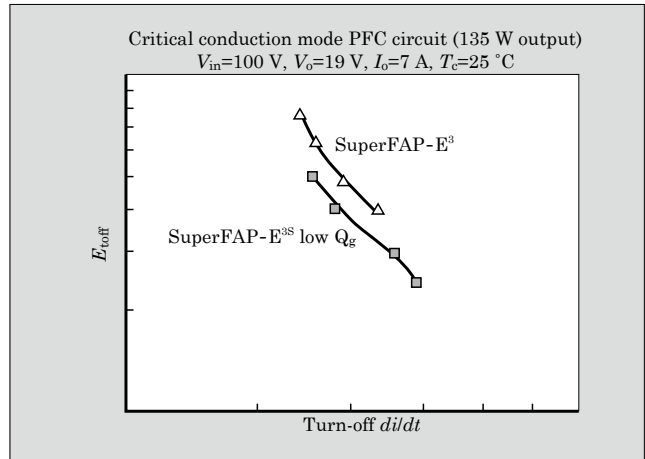
Fig.5 Turn-off loss  $E_{toff}$  vs. turn-off  $dv/dt$



The switching performance improves as a result of reduction of  $Q_g$  and  $g_{fs}$ , and Fig. 5 shows the tradeoff relation between turn-off loss  $E_{toff}$  and turn-off  $dv/dt$ , a cause of noise at switching.

While keeping the same gate resistance controllability as in the prior product series, the tradeoff between turn-off loss  $E_{toff}$  and the drain-source voltage change rate  $dv/dt$  at turn-off is improved by approximately 25% for the same  $dv/dt$  conditions. Also, as shown in Fig. 6, the tradeoff relation between the current change rate  $di/dt$  at turn-off and the turn-off loss

Fig.6 Turn-off loss  $E_{toff}$  vs. turn-off  $di/dt$



improves and better switching performance is realized.

## 4. Application Results

### 4.1 Application to continuous and critical mode PFC circuits

Figure 7 shows waveforms at turn-off in a critical mode PFC circuit. The SuperFAP-E<sup>3S</sup> low  $Q_g$  product has a shorter turn-off interval  $t_{off}$  due to its low gate charge characteristics and realizes approximately 20% less switching loss than the prior SuperFAP-E<sup>3</sup> product.

Figure 8 shows the results of analysis of the generated loss of a continuous mode PFC circuit and of a critical conduction mode PFC circuit in actual applications. In the figure,  $P_{on}$  indicates the on-resistance loss,  $P_{toff}$  indicates the turn-off loss, and  $P_{ton}$  indicates the turn-on loss. In the continuous mode PFC circuit, as in the critical mode PFC circuit, the turn-off loss is reduced by approximately 20% compared to the SuperFAP-E<sup>3</sup> product. Moreover, each circuit results in an approximately 17% reduction in total loss by the effect of the reduction in turn-off loss, and as shown in Table 3, a decrease in the device temperature rise by approximately 4 to 6 °C and an improvement in power conversion efficiency  $\eta$  by approximately +0.4%, as compared to the SuperFAP-E<sup>3</sup> product, enable improved performance of a power supply system.

### 4.2 Application to flyback circuit

Figure 9 shows the effect of reducing rush current at turn-on, which is one cause of noise in a flyback circuit. With the prior SuperFAP-E<sup>3</sup> product, in order to suppress rush current, the gate resistance had to be set to a value approximately 20% larger than that of the SuperFAP-E<sup>3S</sup> low  $Q_g$  product and the turn-on loss increased as a result. The SuperFAP-E<sup>3S</sup> low  $Q_g$  product, however, realizes low turn-on loss and the same or lower rush current as the prior SuperFAP-E<sup>3</sup> product which has a large gate resistance. By applying this SuperFAP-E<sup>3S</sup> low  $Q_g$  product to a flyback circuit, the

Fig.7 Comparison of turn-off waveforms in critical conduction mode PFC circuit

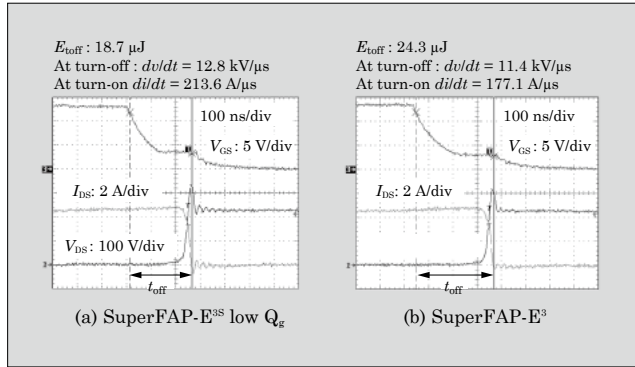
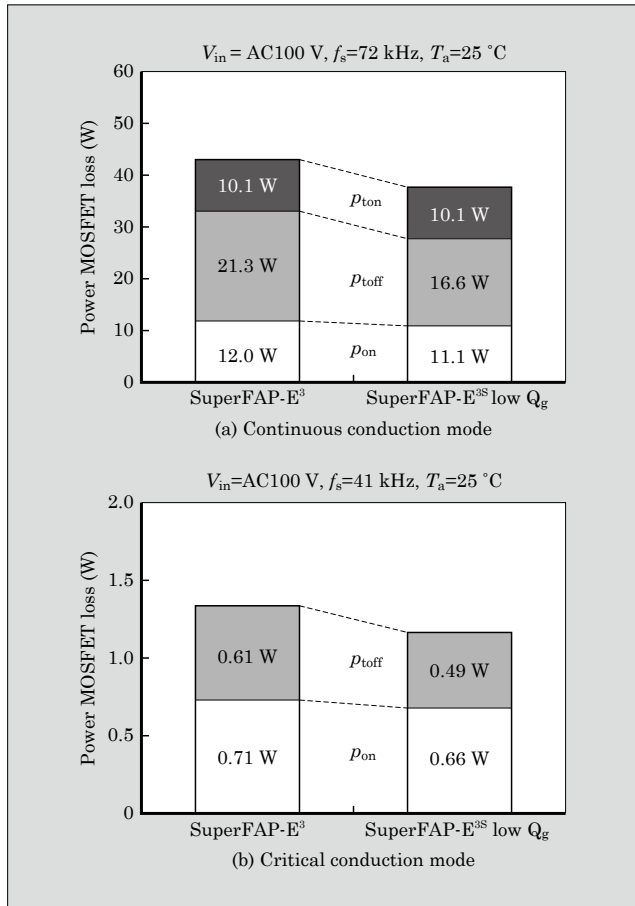


Fig.8 Result of analysis of loss in PFC circuit



noise caused by rush current is reduced and the lower loss is realized.

Figure 10 shows the results of analysis of the loss when using the SuperFAP-E³S low  $Q_g$  product. The lower turn-on and turn-off loss of the SuperFAP-E³S low  $Q_g$  product enable an approximate 12% reduction in total loss compared to the prior product series. An approximate 6 °C reduction in the device temperature rise and an approximate +0.4% improvement in power conversion efficiency  $\eta$  enable the realization of improved performance of the power supply system.

Table 3 Effects of applied new circuit and method

| Application           | Applied circuit and method               | Item                               | Present product | New product | Improvement effect |
|-----------------------|--|------------------------------------|-----------------|-------------|--------------------|
| AC adapter 135 W      | PFC circuit (critical conduction mode)   | Power efficiency $\eta$            | 86.7 %          | 87.1 %      | +0.4 %             |
|                       |  | Case temperature rise $\Delta T_c$ | 34 °C           | 30 °C       | -4 °C              |
| PC power supply 400 W | PFC circuit (continuous conduction mode) | Power efficiency $\eta$            | 72.9 %          | 73.3 %      | +0.4 %             |
|                       |  | Case temperature rise $\Delta T_c$ | 98 °C           | 92 °C       | -6 °C              |
| AC adapter 65 W       | Main converter (flyback)                 | Power efficiency $\eta$            | 87.3 %          | 87.7 %      | +0.4 %             |
|                       |  | Case temperature rise $\Delta T_c$ | 90 °C           | 84 °C       | -6 °C              |

Fig.9 Comparison of turn-on characteristics in flyback circuit

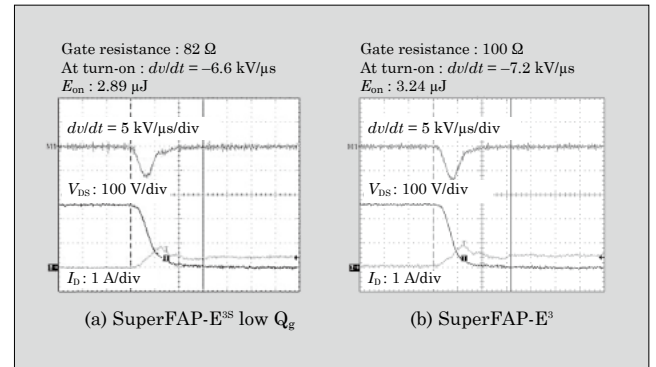
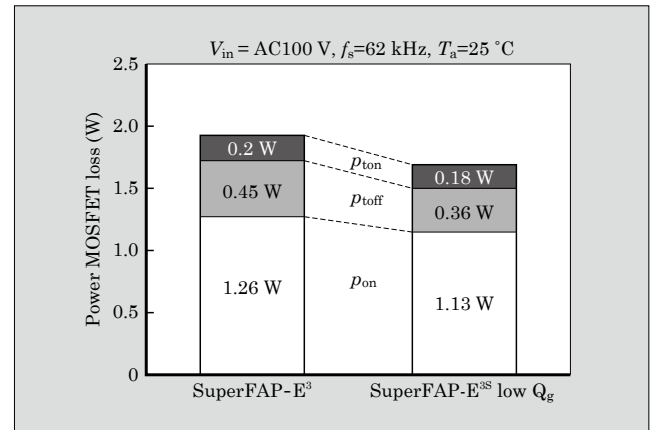


Fig.10 Result of analysis of loss in flyback circuit



## 5. Postscript

This paper has described the product characteristics and application results of Fuji Electric's newly developed SuperFAP-E³S low  $Q_g$  series of power MOSFETs that realize improved switching performance due to lower gate charge characteristics. The SuperFAP-E³S low  $Q_g$  product series achieves a balanced tradeoff between low on-resistance, low switching loss and low noise, which are requested of power

devices installed in switching-mode power supplies, and when used in applications, realizes improved power efficiency and lower temperature rise of electronic device systems, and can contribute to energy savings.

#### Reference

- (1) Kobayashi, T. et al. High-voltage Power MOSFETs Reached Almost to the Silicon Limit. Proceedings of ISPSD '01.2001. p. 435-438.





# SMD-type Small Atmospheric Pressure Sensor for High-altitude Compensation

Kazunori Saito <sup>†</sup>  
Kimihiro Ashino <sup>†</sup>  
Shojiro Kurimata <sup>†</sup>

## 1. Introduction

The environmental activities in the automotive industry are increasing while the environmental regulations are tightened in Europe, United States, Japan, Asia environmental and else where throughout the world. In order to comply with such regulations, automobile systems are becoming more efficient and are realizing higher control accuracy. Moreover, the engine management functions that measure and control pressure in these systems have become increasingly important in recent years.

Fuji Electric has been mass-producing automobile pressure sensors since 1984. Responding to severe changing needs for lower cost and higher precision, Fuji Electric has proposed proprietary high reliability circuit technology and advanced MEMS (micro electro mechanical systems) technology that is being used in automobiles and motorcycles both in Japan and overseas. Since 2007, Fuji Electric has been mass-producing 5th generation digital trimming type automotive pressure sensors using a CMOS (complementary metal-oxide-semiconductor) process.

This paper introduces a SMD (surface mount device)-type small pressure sensor that has been developed using a 5th generation digital trimming type automotive pressure sensor chip and that can be mounted onto the surface of an ECU (electronic control unit) circuit board and used for high-altitude compensation when an automobile travels at high elevations.

## 2. Use for Atmospheric Sensors

Automotive pressure sensors are generally used in the electronic fuel injection system of a combustion engine to measure pressure inside the intake manifold in order to control the air-fuel ratio optimally. On the other hand, in order to compensate for error in the air-fuel ratio primarily at high elevations, atmospheric pressure sensors are used to measure the atmospheric pressure and to control the air-fuel ratio in consideration of the lack of oxygen due to thin air when travel-

ing at high elevations. The basic specifications and appearance of Fuji Electric's newly developed atmospheric pressure sensor are shown in Table 1 and Fig. 1, respectively.

Table 1 Basic specifications of the atmospheric pressure sensor

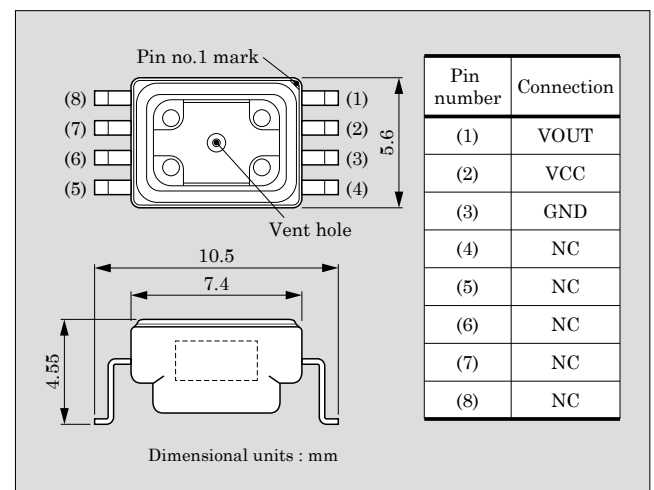
| Item  | Specification                                    | Remarks |
|---|--|---------|
| Absolute max. voltage                         | 16.5 V   | < 1min  |
| Absolute max. pressure                        | 490 kPa abs                                      |         |
| Storage temperature                           | -40 to + 110 °C                                  |         |
| Usage temperature                             | -30 to + 105 °C                                  |         |
| Usage pressure                                | 50 to 120 kPa abs                                | *3      |
| Output range                                  | 0.5 to 4.5 V                                     |         |
| Interface                                     | PU <sup>*1</sup> 300 kΩ, PD <sup>*2</sup> 100 kΩ |         |
| Diag area                                     | < 0.2 V, >4.8 V                                  | *4      |
| Sink current                                  | 1 mA   |         |
| Source current                                | 0.1 mA   |         |
| Pressure error                                | < 3.0 %FS  |         |
| Temperature error                             | < 1.5×   |         |
| Electro-magnetic compatibility (EMC) standard | JASO D00-87, CISPR 25, ISO 11452-2, ISO7637      |         |

\*1 : Pull Up      \*2 : Pull Down

\*3 : Relative pressure and full-scale pressure can be changed arbitrarily

\*4 : Detection of disconnected VCC wiring or VOUT wiring

Fig.1 Appearance of atmospheric pressure sensor



<sup>†</sup> Fuji Electric Device Technology Co., Ltd.

### 3. Package Design Technology for a Small Atmospheric Pressure Sensor

#### 3.1 Miniaturized design

For board-mounted parts, the miniaturization of package sizes has the result of reducing the required mounting area, thereby enabling a reduction in the total area of the circuit board, and as a factor that greatly affects the overall cost of the ECU product, miniaturization is an essential aspect of the package development stage. To realize a miniaturized package, the resin thickness of the package was reduced, and the bonding inner terminal was made narrower, and the pin pitch was also made narrower (1.27 mm) to achieve ultra miniaturization. Compared to a conventional package having the dimensions of 11.5 mm (length) × 11.5 mm (width) × 6.6 mm (thickness), the new package dimensions are 6.5 mm (length) × 7.4 mm (width) × 4.05 mm (thickness), and consequently, the mounting area has been reduced by approximately 65% compared to the conventional package, and the packaging volume, which includes the height dimension, was also reduced by approximately 76%. Figure 2 compares the appearance and size of the conventional package and

Fig.2 Comparison of conventional intake pressure sensor and atmospheric pressure sensor

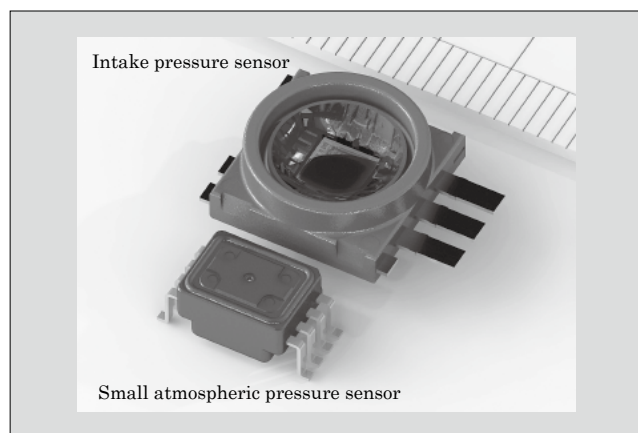
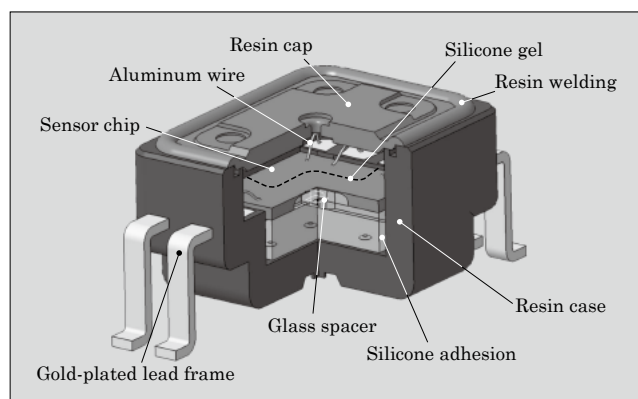


Fig.3 Cross-sectional structure of atmospheric pressure sensor



the new package.

The internal structure of the atmospheric pressure sensor has the same basic configuration as a conventional product but is additionally provided with a resin cap for protecting a gold-plated lead frame used for the purpose of soldering to the ECU circuit board and for protecting the chip (silicon gel) surface. Figure 3 shows the cross-sectional structure of this atmospheric pressure sensor.

#### 3.2 Package analysis technology

Because a pressure sensor is a semiconductor element that senses pressure as stress and converts that stress value into an electric signal, it can also be called a “stress sensor.” Being sensitive to stress, the temperature characteristics, offset voltage and other sensor characteristics may be affected by various stresses

Fig.4 FEM analysis examples

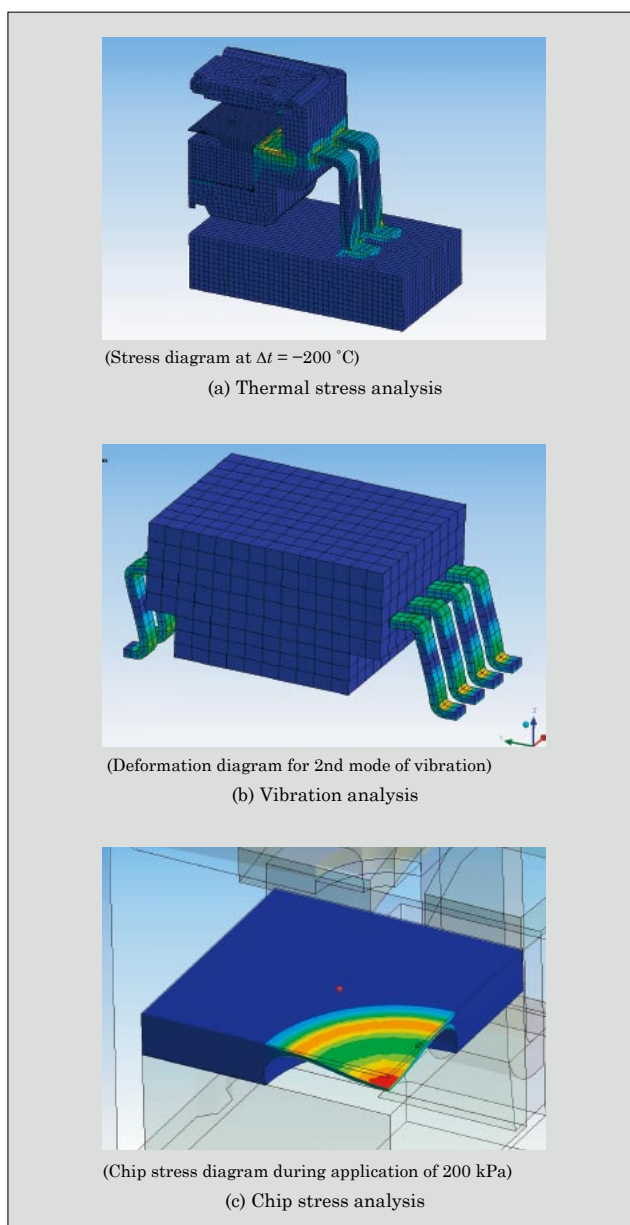
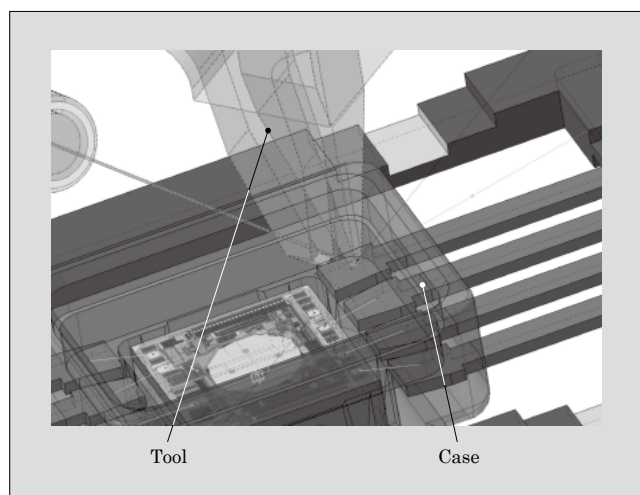


Fig.5 Example of bonding interference simulation



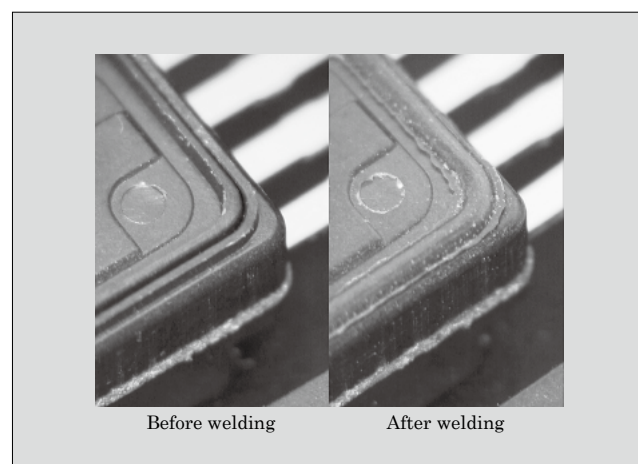
received from the package. Accordingly, a key factor of the package design is the extent to which the structure prevents stress from being transferred to the chip. For this purpose, FEM (finite element method) analysis is extremely important so that the package stress can be analyzed in advance and the package structure optimized. The analyses actually performed include vibration analysis, pressure resistance analysis, terminal drawing strength, chip stress analysis, and so on. Here, examples of thermal stress analysis, vibration analysis and chip stress analysis are shown in Fig. 4.

### 3.3 Assembly design technology

#### (1) Aluminum wire bonding

The pressure sensor package is designed in consideration of interference that may arise between the package and the bonding tool when bonding aluminum wire during the assembly process. As a consequence of the reduction in size of the bonding area due to the package miniaturization, the extremely close proximity of the bonding tool increases the risk of interference. Therefore, during the design stage, care must be taken to prevent such interference from leading to bonding defects. The product is designed using 3-dimensional CAD (computer aided design), and during the design stage, using a CAD-generated model as shown in Fig. 5, a modeled tool reproduces the bonding operation by tracing the actual bonding path between the chip and the package bonding areas so as to check for interfer-

Fig.6 Comparison of appearance before and after impulse welding



ence with the package and to avoid the risk of interference during assembly.

#### (2) Cap joining

Impulse welding technology is used for joining together the cap and case. Impulse welding is a heat welding technique that forms tight joints by quickly heating resin so that it melts and then quickly cooling the resin so that it becomes fixed.

With the conventional method in which an adhesive agent was used to join the cap to the case, because the package had been miniaturized it was difficult to ensure a sufficient adherence margin, and adequate air tightness and adhesion strength were difficult to obtain. However, as shown in Fig. 6, the use of the impulse welding technology enabled these problems to be solved.

## 4. Postscript

This paper has presented an overview of Fuji Electric's small atmospheric pressure sensor for automobiles. As interest in environmental conservation intensifies and as the systems that control automobiles achieve higher levels of sophistication and performance, the requirements for pressure sensors are expected to become increasingly severe. In the future, Fuji Electric intends to develop products having even higher accuracy and higher quality, and will strive to develop the highest level of technology in the world.



# Modeling of Conduction EMI Noise and Technology for Noise Reduction

Shuangching Chen <sup>†</sup>  
Taku Takaku <sup>†</sup>  
Seiki Igarashi <sup>†</sup>

## 1. Introduction

With the recent advances in high-speed power semiconductor devices, the trends toward increased carrier frequencies and smaller-size inverters are advancing. High-frequency switching, however, is associated with the problem of high-frequency leakage current flowing through the stray capacitance of the motor windings to the grounding wire and the problem of EMI (electromagnetic interference). The following three methods are being considered for reducing conduction noise which is a problem in the frequency range of 150 kHz to 30 MHz.

- (a) Passive method<sup>(1)</sup>: Configured from passive components only. The leakage current is suppressed by inserting passive filter in the common-mode current path. This method has the disadvantages, however, of not enabling a reduction in coil size and of requiring a motor neutral point.
- (b) Active EMI filter<sup>(2)</sup>: Injects current having an opposite phase from that of the control current source in order to cancel the leakage current to the power supply. When a long cable is used, this method has the disadvantages of a large leakage current and of requiring large components for grounding.
- (c) Active common noise canceller<sup>(3)</sup>: Superimposes a voltage from the control voltage source that is opposite the common-mode voltage in order to cancel the common-mode voltage. This method has the disadvantages of a large transformer size due to 2-arm modulation. Because the stray capacitance of the heat sink is not considered, the inability to completely prevent noise from entering the power source.

A reduction in size of the conduction EMI filter is difficult to achieve, with the passive method and the active EMI filter method. Fuji Electric's research focused on the active common-mode canceller, and an improved low voltage-type and small size active filter was devised.

Meanwhile, advances in computer technology and

simulation technology have enabled realistic modeling of conduction noise and the highly accurate prediction of noise levels<sup>(4), (5)</sup>. As a result, various analyses and noise suppression methods can be considered within a short time.

This paper describes the modeling of conduction noise, the simulation-based analysis of noise reduction technologies, and experimental results of the noise reduction effect in improved active common-mode canceller.

## 2. Modeling of Conduction EMI Noise

### 2.1 Measurement of common-mode leakage current

Figure 1 shows the flow path of common-mode leakage current in the motor drive inverter system. The common-mode leakage current can be categorized as motor leakage current, module leakage current through a copper base, leakage current through a grounding capacitor, and power source (line impedance stabilization network: LISN) leakage current. In this research, a

Fig.1 Block diagram of measurement circuit for conduction EMI noise

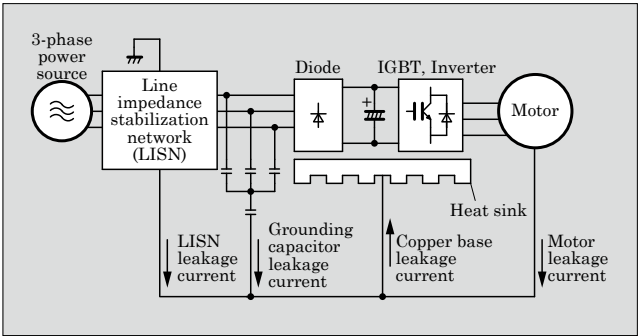


Table 1 Test conditions and test equipment

|                              |                          |
|------------------------------|--------------------------|
| IGBT module                  | 6MBI75U2A-060            |
| Motor                        | 2.2 kW, 200 V            |
| Cable between IGBT and motor | 2 mm <sup>2</sup> , 10 m |
| DC bus voltage               | 140 V or 280 V           |
| LISN                         | Kyoritsu Corp. KNW-243C  |
| Spectrum analyzer            | Advantest R3261          |

<sup>†</sup> Fuji Electric Device Technology Co., Ltd.

15 kW/200 V inverter system was simulated, and the leakage current was measured with a chopper circuit using Fuji Electric's IGBT module 6MBI75U2A-060. A 200 V, 2.2 kW motor was used as the load.

Table 1 lists the test conditions and the test equipment used for measuring the common-mode leakage current. Under the conditions specified in Table 1, the common-mode leakage current waveform was measured for a switching operation, and a high frequency equivalent circuit was derived from the resonant frequency of each current waveform.

## 2.2 Modeling of motor leakage current

Figure 2 shows actually measured leakage current waveforms for a DC bus voltage of 140 V.

An equivalent circuit for the high-frequency leakage current can be expressed with an LCR series resonant circuit. The equivalent circuit of the leakage current can be considered to be configured as two LCR series resonant circuits connected in parallel as shown in Fig. 3. The  $L$  and  $C$  values in the resonant circuit can be determined from the natural resonance angular frequency  $\omega_n$  and the characteristic impedance  $Z_0$  ac-

Fig.2 Measured leakage current waveform (DC bus voltage: 140 V)

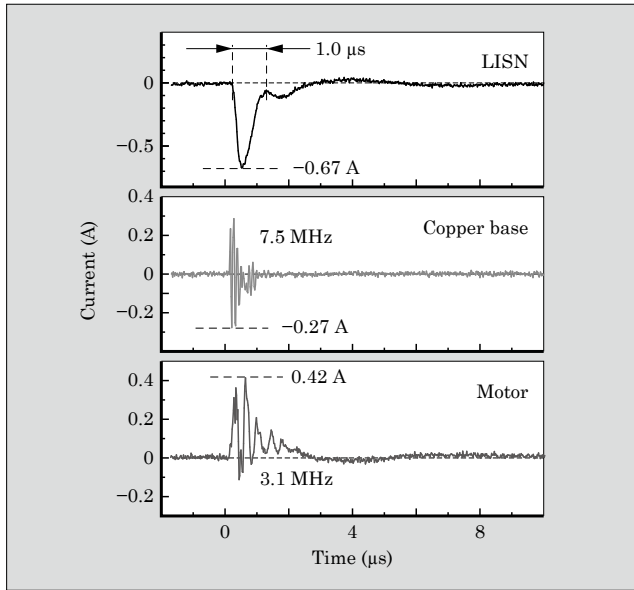
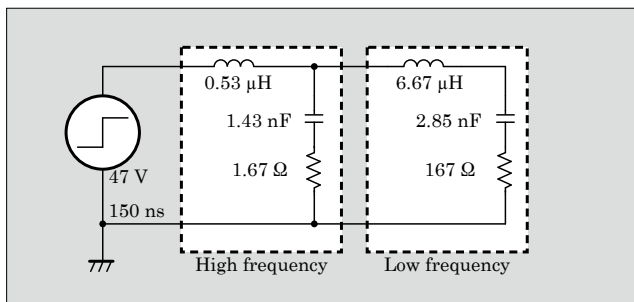


Fig.3 Equivalent circuit of motor common-mode leakage current



ording to the following formulas.

$$L = Z_0 / \omega_n, C = 1 / \omega_n Z_0 \quad (1)$$

$R$  is determined from the attenuation of the envelope curve. Because the high-frequency amplitude is greatly affected by the common-mode voltage of the inverter, the measured line inductance of 0.53 μH at 100 kHz is used as the high frequency component inductance.

Figure 4 shows a circuit in which the common-mode leakage current of the motor has been replaced by a 3-phase equivalent circuit<sup>(4)</sup>. When replacing a single-phase equivalent circuit with a 3-phase equivalent circuit, the low-frequency component inductance and the resistance values are tripled. Also, in consideration of the inductance of the grounding wire, the high-frequency component inductance of the 3-phase equivalent circuit is 3/4 of the single-phase inductance. Moreover, each capacitance is separated into a grounding capacitance  $C_g$  and a motor stray capacitance  $C_m$ .

## 2.3 Modeling of the entire circuit

Figure 5 shows a PSIM<sup>\*1</sup> simulation circuit that models conduction leakage current. The circuit constants are computed as follows.

- Copper base stray capacitance: This is the stray capacitance between semiconductor devices and the copper base, and is 200 pF per device, with the inverter using 6 devices.
- Heat sink inductance and resistance value: Computed from an actual measured waveform of the copper base leakage current and from the copper base stray capacitance.
- Motor equivalent circuit: The attenuated oscillatory waveform of the measured motor leakage current is separated into a high frequency component and a low frequency component, and circuit constants are computed from a LCR series resonance circuit.
- Grounding capacitor: The capacitance used is converted into a single-phase equivalent circuit.

\*1: PSIM is Myway Labs' simulation tool for power electronics circuit.

Fig.4 3-phase equivalent circuit of motor common-mode leakage current

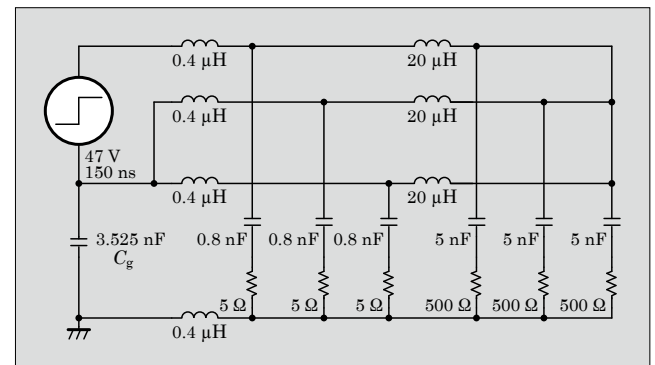




Fig.5 PSIM simulation model (chopper circuit)

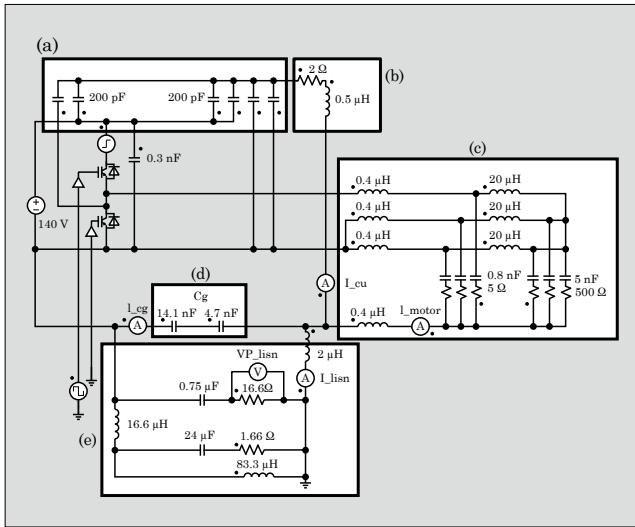
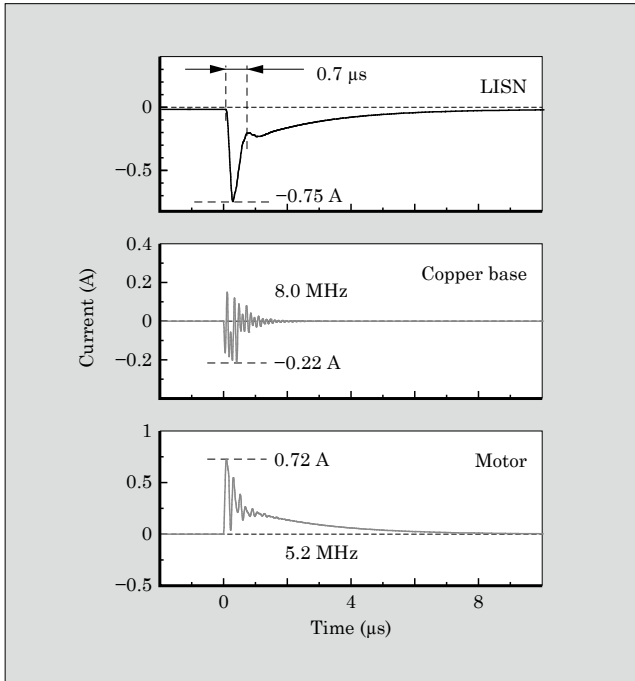


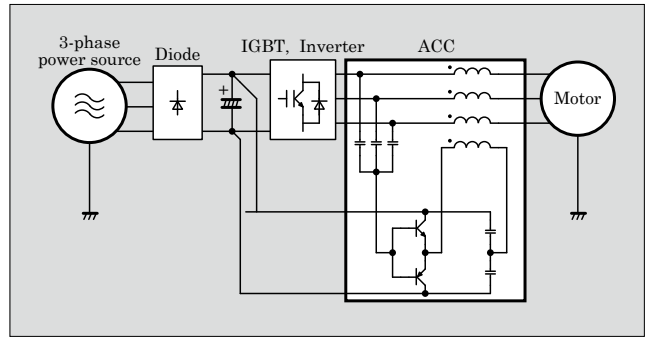
Fig.6 Simulated leakage current waveform (DC bus voltage: 140 V)



(e) LISN: A 3-phase circuit is converted into a single-phase equivalent circuit.

Figure 6 shows simulated leakage current waveforms obtained using the PSIM simulator with DC bus voltage set to 140 V. The peak value of measured LISN leakage current shown in Fig. 2 was -0.67 A, and the simulated LISN leakage current had a peak value of -0.75 A. Moreover, there is close agreement between the measured and simulated values of the frequencies and peak values of copper base leakage current and the motor leakage current. From these results, we conclude that conduction EMI noise can be modeled and that simulation-based analysis is feasible.

Fig.7 ACC circuit configuration



### 3. Noise Reduction Technology and Effect

#### 3.1 Voltage type active common-mode canceller

The passive filter built into an inverter occupies approximately 30% of the total volume of that inverter. In order to further reduce the volume of the inverter, the filter must be miniaturized. In our research, we propose an improved low-voltage active filter to reduce the size of the EMI filter, so that it may be incorporated into an inverter.

The active common-mode canceller (ACC) shown in Fig. 7 is a method that was proposed by Ogasawara et al<sup>(3)</sup>. With this method, a voltage, opposite in polarity to and having an amplitude approximately equal that of the common-mode voltage fluctuations generated by switching, is injected between the inverter output and the motor, and cancels the common-mode voltage fluctuations to enable the removal of leakage current generated on the motor side. However, the common-mode voltage between the inverter and the LISN is not cancelled. Therefore leakage current flows to the power source through module copper base and grounding capacitor. This method has a disadvantage that the high voltage transistor is required because the power supply for the compensation voltage source is DC bus of the inverter.

#### 3.2 Low voltage active filter

When one phase of the inverter is switched, the common-mode voltage changes by 1/3 of the DC bus voltage  $E_{dc}$ . Because the stray capacitance of the inverter is extremely small compared to the stray capacitance of the motor, the common-mode equivalent circuit can be considered to be a series circuit of the grounding capacitance  $C_g$  and the motor stray capacitance  $C_m$ . Thus, the amplitude of the voltage fluctuations generated across the grounding capacitance is  $E_d/3$  voltage-divided by  $C_g$  and  $C_m$ . Limiting the suppression of the LISN leakage current makes it possible to reduce the voltage to be compensated and enables the ACC that generates voltages of opposite polarity to be configured from low-voltage active devices.

Figure 8 shows the proposed low voltage ACC circuit configuration. A common-mode transformer is inserted between the LISN and the inverter. Common-

Fig.8 Proposed low-voltage ACC method

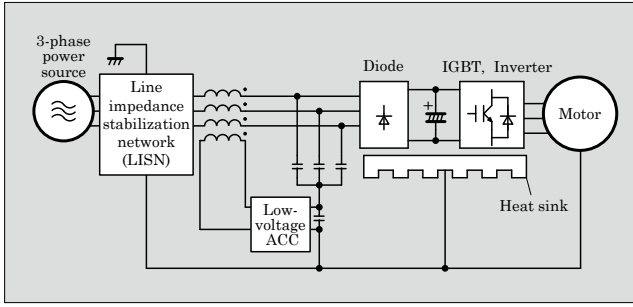
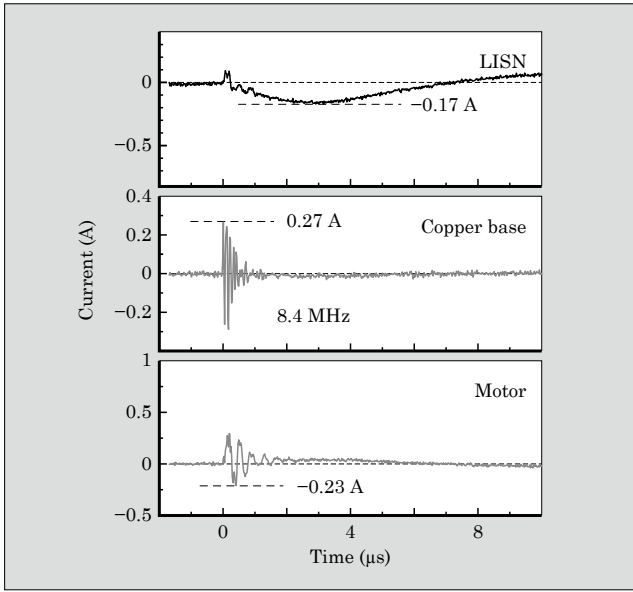


Fig.9 Measured waveform of leakage current with ACC (DC bus voltage: 140 V)



mode voltage fluctuation of the grounding capacitance is detected, and a voltage of the opposite phase is applied by the common-mode transformer. As a result, in principle, the leakage current flowing to the power source side can be suppressed entirely. Moreover, because the voltage outputted by the ACC circuit is only the voltage divided between the grounding capacitance and the motor stray capacitance, the circuitry can be configured from lower voltage parts than in a conventional ACC circuit. Since low voltage parts generally have excellent high-frequency characteristics, it is possible to compensate higher frequency component. Moreover, because their cost is low, a noise filter can be configured inexpensively. Additionally, because the compensating voltage can be reduced, the transformer is unlikely to saturate magnetic flux and the common-mode transformer can be miniaturized.

### 3.3 Experimental result

Figure 9 shows the measured waveforms of leakage currents when a low-voltage ACC circuit is combined with a chopper circuit that uses the parameters shown in Table 1. The peak value of LISN leakage current with ACC was reduced to approximately a quarter of

Fig.10 Simulated waveform with ACC (DC bus voltage: 140 V)

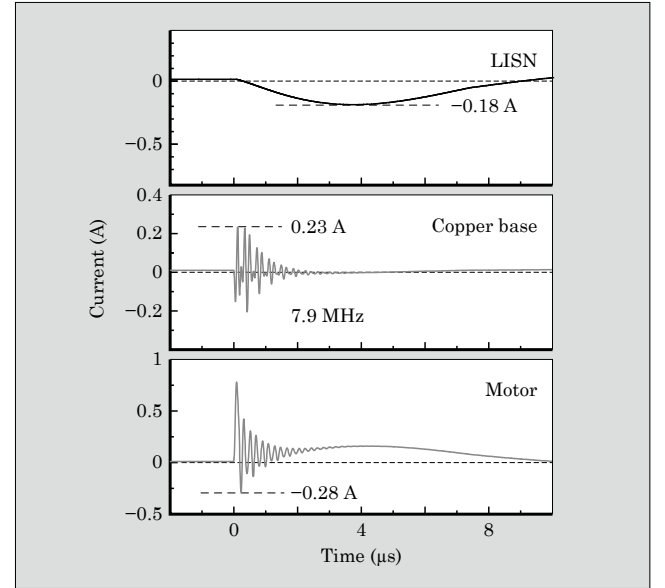
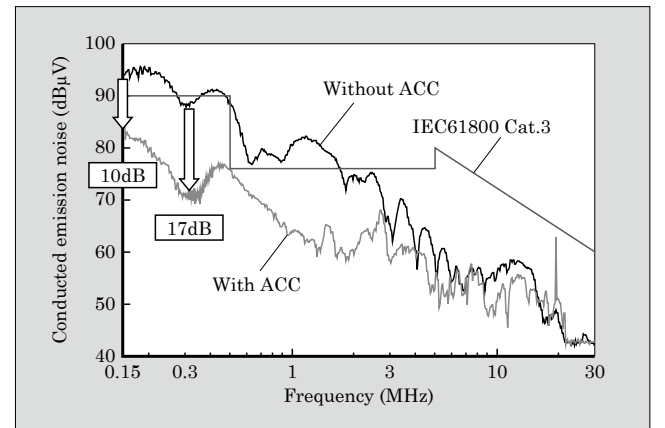


Fig.11 Measured conducted emission noise with and without ACC (DC bus voltage: 280 V)



the peak value shown in Fig. 2.

For the copper base and the motor leakage currents, a large difference was not observed between with and without ACC. The reason is because the proposed method focuses only on the leakage current to the power source. The simulated waveforms under the same conditions are shown in Fig. 10. The simulated results tend to agree closely with the measured data, and the effectiveness of the modeled simulation circuit was verified.

Figure 11 shows the measured results of the conducted emission spectrum, with and without the proposed ACC. The DC bus voltage was set at 280 V. This experiment is a chopper circuit experiment that simulates an inverter, and the conducted emission voltage was lower than in the case of an inverter. In Fig. 11, “without ACC” indicates the conduction noise when there is no filter and “with ACC” indicates the conduction noise when a proposed low voltage ACC has been inserted. With this proposed method, the conducted

emission noise was decreased significantly at frequencies of 3 MHz or lower, at 150 kHz and at 300 kHz, the conducted emission noise was decreased by 10 dB and 17 dB, respectively. At high frequencies above 3 MHz, the noise reduction effect is negligible. The reason for the lack of noise reduction is due to the limited high frequency response of active components such as transistors and op-amps used in the proposed ACC circuit.

#### 4. Postscript

This paper has described the modeling of conduction EMI noise and technology for noise reduction using a low voltage active common-mode filter. We proposed a low voltage ACC circuit that was found to reduce significantly the common-mode noise at the power source. Moreover, the proposed circuit configuration has a lower cost than a conventional noise filter and can be miniaturized. In the future, Fuji Electric intends to make the ACC circuit compatible with integrated circuit technology and to develop a commercial

product.

#### Reference

- (1) Akagi, H. et al. Design and performance of a passive EMI filter for use with a voltage-source PWM inverter having sinusoidal output voltage and zero common-mode voltage. *IEEE Transaction on Power Electronics*. Vol. 19, no. 4, 2004, p. 1069-1076.
- (2) Ogata, A. et al. Active compensation circuit of leak current in inverter driven load. 1996 National convention record IEEJ, no. 852.
- (3) Ogasawara, S. et al. Active cancellation of the common-mode voltage produced by a voltage-source PWM inverter. *IEEJ D*, vol. 117, no. 5, 1997, p.565-571.
- (4) Aoki, M. et al. Frequency analysis of conduction EMI generated by a PWM inverter. *SPC-07-17*, p. 37-42.
- (5) Ogasawara, S., Akagi, H. Modeling and damping of high-frequency leakage currents in PWM inverter-fed AC motor drive systems. *IEEE*. Vol. 32, no. 5, Sep/Oct 1996, p. 1105-1114.



# Technology for Controlling Trench Shape in SiC Power MOSFETs

Yasuyuki Kawada<sup>†</sup>  
Takeshi Tawara<sup>†</sup>  
Shun-ichi Nakamura<sup>†</sup>

## 1. Introduction

As the worldwide consumption of energy is increases and the global environment steadily deteriorates, society must find more efficient ways to utilize energy in order to achieve sustainable advances. Accordingly, the field of power electronics is of vital importance, and huge advances in power semiconductor devices are anticipated. Power semiconductor devices that use silicon (Si) are said to be approaching the limits of their inherent characteristics, and although technical developments such as the SJ-MOSFET (super junction metal-oxide-semiconductor field-effect transistor) and FS-IGBT (field stop insulated gate bipolar transistor) have resulted in improved characteristics, further improvement will be difficult to realize. Silicon carbide (SiC), a compound that combines silicon and carbon, has physical properties that are superior to those of Si, and is capable of achieving high voltage, low on-resistance, low loss and high-speed operation. The application of SiC devices enables power supplies to be made smaller in size, have lower loss, operate at high temperatures (with a simplified the cooling mechanism), and also enables electric power energy to be utilized more effectively.

As devices that use SiC material, some Schottky barrier diodes are being sold commercially, and as switching devices, MOSFETs have been much researched, but are not yet being used in practical applications. Trench-type MOSFET (UMOSFET) devices promise to realize lower on-resistance than the planar types, but require SiC-specific dry etching technology. Being physically hard and chemically stable, SiC material is difficult to etch, and even with an etching machine that uses high density plasma, the etching rate is slow and the etching shape is difficult to control. A trench sidewall or bottom surface formed by dry etching exhibits surface roughness and areas with sharp angles remain at the opening portion. In a UMOSFET, because a channel is formed in the trench sidewall, the smoothness affects electron mobility and the presence of sharp angles in the trench invites decreased

withstand voltage capability due to the concentration of electric fields. Thus, smoothing of the trench inner wall and rounding of the corner shapes of the trench opening and bottom are essential. However, it is difficult to obtain an ideal shape and smoothness by only optimizing the dry etching conditions.

On the other hand, high-temperature annealing in a hydrogen (H<sub>2</sub>) atmosphere is known to improve the trench shape and smoothness of Si trench devices.<sup>(1)(2)</sup> SiC is also stable at high temperatures, and there have been no reports of this type of approach applied to SiC. This paper examines technology for simultaneously performing high-temperature annealing of SiC trenches and performing process optimization in order to control trench shape and improve sidewall smoothness.

## 2. Experimental Procedure

A sample was prepared by forming SiO<sub>2</sub> film at a thickness of 2 μm on a 4H-SiC (see explanatory note on page 73) substrate (8° off the C face), and then patterning the resist with a line width of 1 to 3 μm. Next, the resist was worked as a mask and dry etching was performed to pattern the SiO<sub>2</sub>. After the resist was removed, the SiO<sub>2</sub> worked as a mask and then the SiC was dry etched. The etching depth ranged from 3 to 8 μm. After hydrofluoric acid was used to remove the SiO<sub>2</sub> film, annealing was performed for 1 to 30 minutes in an atmosphere of argon (Ar), silane-added argon (SiH<sub>4</sub>/Ar) and hydrogen (H<sub>2</sub>) at 1.5 to 760 Torr using a CVD (chemical vapor deposition) apparatus capable of achieving temperatures of up to approximately 2,200 °C. For evaluation purposes, a scanning electron microscopy (SEM) was used to observe the trench inner wall and a cross-section thereof before and after the annealing, and an atomic force microscope (AFM) was used to measure the substrate surface roughness and the roughness of the trench sidewall. For some samples, X-ray photoelectron spectroscopy (XPS) was used to analyze Si and C binding and composition on the substrate surface.

<sup>†</sup> Fuji Electric Device Technology Co., Ltd.

### 3. Results and Considerations

#### 3.1 Pressure dependency of annealing

Figure 1 shows cross-sectional and plane surface SEM photographs of trenches annealed in an Ar atmosphere at 1,700 °C at the different pressures of 1.5 Torr, 80 Torr and 760 Torr.

Figure 1(a) shows the cross-section and bottom of a trench that has not been annealed after the trench etching. It can be seen that without annealing, the corners of the trench opening are formed from nearly right-angles, and the trench bottom is rough. In the case of annealing at 1,700 °C in an Ar atmosphere at 1.5 Torr, the trench shape and the trench bottom surface exhibit little change, but at 80 Torr and 760 Torr, the corners of the trench opening become rounded and the trench bottom becomes smooth.

Figure 2 shows the XPS measurement results for carbon at the substrate surface of these samples. For the sample without annealing and those with annealing at 80 Torr and 760 Torr, a peak binding energy due to the SiC was observed, but for the sample annealed

Fig.1 Pressure dependency of shape of SiC trench annealed in an Ar atmosphere at 1,700 °C

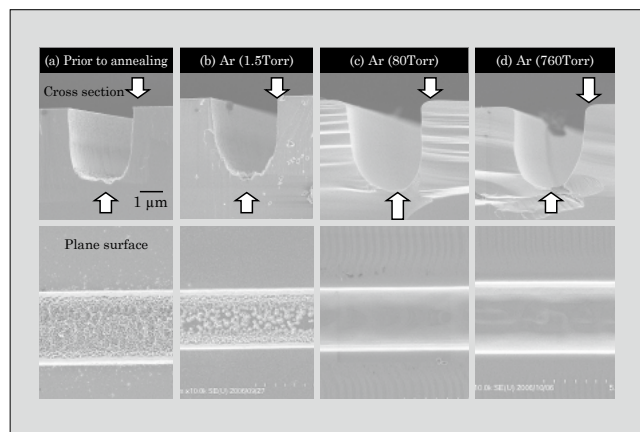
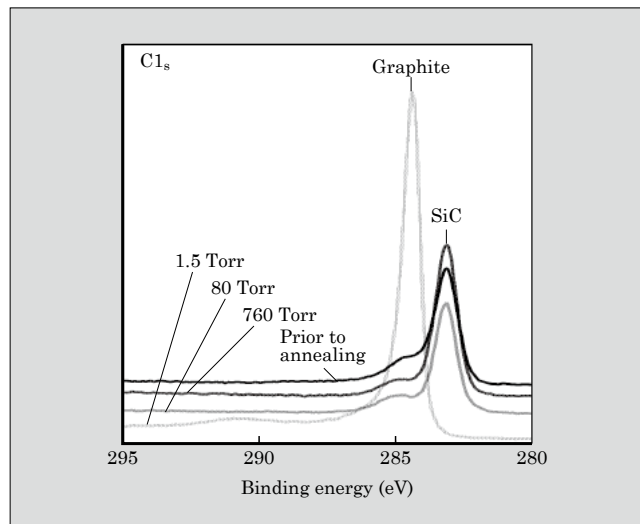


Fig.2 XPS measurement results of C1s peak on SiC surface



at 1.5 Torr, the binding energy peak was shifted toward the high energy side. This shifted peak is for graphite, confirming that when annealing is performed at 1.5 Torr, the Si sublimates from the substrate surface and the surface becomes nearly entirely composed of C. Based on these results, we found that improvements in the trench shape and smoothness could not be realized at low pressures, and that a suitable annealing pressure is at least 80 Torr. Subsequent experiments were conducted at 80 Torr.

#### 3.2 Dependency on annealing atmosphere

Figure 3 shows cross-sectional and plane surface SEM photographs of trenches annealed at a temperature of 1,700 °C, a pressure of 80 Torr and in the different annealing atmospheres of Ar, SiH<sub>4</sub>/Ar and H<sub>2</sub>.

The samples annealed in atmospheres of Ar and SiH<sub>4</sub>/Ar exhibited rounded trench corners and smooth trench bottoms. However, the sample annealed in a H<sub>2</sub> atmosphere had a smooth trench bottom, but areas in the vicinity of the trench opening and sidewall exhibited signs of significant etching.<sup>(3)</sup> Due to the significant trench sidewall etching that occurs during annealing in a H<sub>2</sub> atmosphere at 1,700 °C, temperature optimization is required. Optimization of the annealing temperature was examined below for the cases of annealing in a SiH<sub>4</sub>/Ar atmosphere and in a H<sub>2</sub> atmosphere.

#### 3.3 Temperature dependency of annealing in a SiH<sub>4</sub>/Ar atmosphere

Figure 4 shows cross-sectional and plane surface SEM photographs of trenches annealed in a SiH<sub>4</sub>/Ar atmosphere at 80 Torr at various temperatures ranging between 1,500 °C and 1,800 °C.

As the annealing temperature rises, the corners of the trench opening become more rounded, and surface roughness on the trench bottom decreases and becomes smoother. In order to make the trench corners become rounded, a temperature of at least 1,700 °C is required. In the plane surface SEM photographs, step bunching (a phenomenon of waviness caused by an aggregation of atomic steps) was observed in substrate surfaces

Fig.3 Atmosphere dependency of shape of SiC trench annealed at 1,700 °C

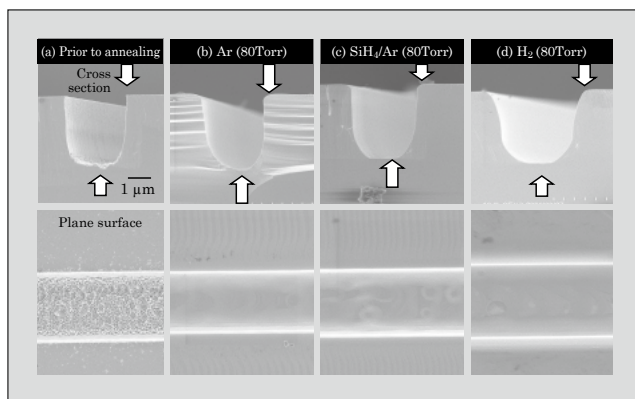




Fig.4 Temperature dependency of SiC trench shape with annealing in SiH<sub>4</sub>/Ar atmosphere

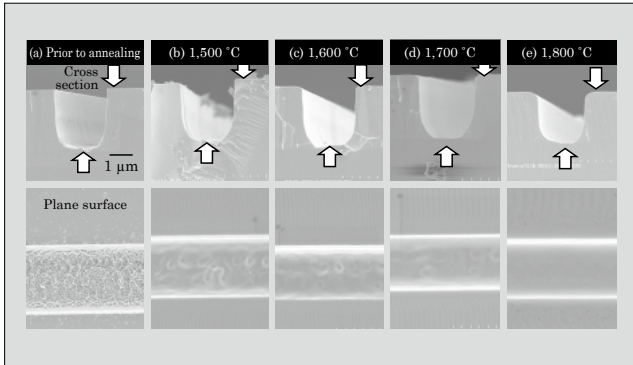
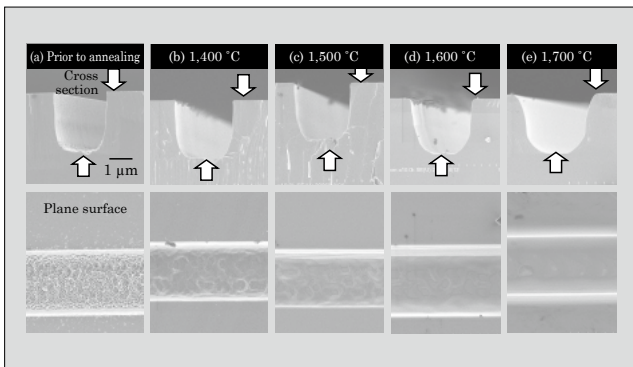


Fig.5 Temperature dependency of SiC trench shape with annealing in H<sub>2</sub> atmosphere



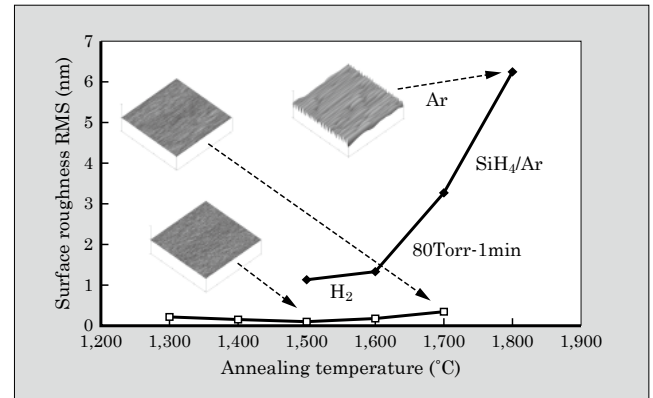
that had been annealed at temperatures of 1,700 °C or higher. This step bunching is believed to be due to an 8° offset of the substrate, and is caused by the release of strain incurred during polishing as a result of the annealing. Measurement of the roughness of the substrate surface with an AFM indicated greater roughness as the annealing temperature increased. From these results, we found that an annealing temperature of 1,700 °C is suitable for obtaining rounded trench corners, a smooth trench bottom surface and reduced substrate surface roughness.

### 3.4 Temperature dependency of annealing in a H<sub>2</sub> atmosphere

Figure 5 shows cross-sectional and plane surface SEM photographs of trenches annealed in a H<sub>2</sub> atmosphere at 80 Torr at various temperatures ranging between 1,400 °C and 1,700 °C.

We verified that as the annealing temperature increases, the bottom of the trench becomes smoother, but if the annealing is performed at a temperature of 1,600 °C or above, the sidewalls become etched and thereby increase the width of the trench. We also found that rounded trench corners could not be obtained by annealing at temperatures of 1,500 °C and below. Measurement of the roughness of the substrate surface with an AFM revealed a RMS (root mean square) roughness of 0.3 nm or less regardless of the

Fig.6 Surface roughness for various annealing conditions



annealing temperature, and that the annealing did not generate any additional roughness.

### 3.5 Annealing conditions and substrate surface roughness

Figure 6 shows the results of measurement of SiC substrate surface roughness with an AFM in the cases where annealing was performed at various temperatures in Ar, SiH<sub>4</sub>/Ar and H<sub>2</sub> atmospheres. The analysis range is a 10 μm square.

With H<sub>2</sub> annealing, the substrate surface was extremely smooth, even at high annealing temperatures. With SiH<sub>4</sub>/Ar annealing, as the temperature increased, step bunching occurred and RMS deteriorated rapidly. At the same temperature, surface roughness was greatest with Ar annealing.

### 3.6 Results of two-step annealing with SiH<sub>4</sub>/Ar and H<sub>2</sub>

Annealing in a high temperature SiH<sub>4</sub>/Ar atmosphere is effective for obtaining rounded trench corners, and annealing in a low temperature H<sub>2</sub> atmosphere is effective for obtaining a smooth substrate surface without changing the trench shape. Based on these results, we examined the feasibility of annealing in a SiH<sub>4</sub>/Ar atmosphere to obtain rounded trench corners and smooth trench inner walls, and then annealing in a H<sub>2</sub> atmosphere to obtain a smooth substrate surface. Figure 7 shows cross-sectional and plane surface SEM photographs of trenches that have been annealed in two steps, first for 10 minutes at 1,700 °C in a SiH<sub>4</sub>/Ar atmosphere and then for 10 minutes at 1,500 °C in a H<sub>2</sub> atmosphere.

It can be seen that the trench corner is rounded to a radius of curvature of 0.6 μm and that the bottom of the trench is extremely smooth. Measurement of the roughness of the substrate surface with an AFM verified that the RMS roughness has been improved to 1.59 nm. Thus, the consecutive implementation of annealing at 1,700 °C in a SiH<sub>4</sub>/Ar atmosphere and then annealing at 1,500 °C in a H<sub>2</sub> atmosphere enables an improvement in the trench corner shape and substrate smoothness.

Using an SEM and AFM, the smoothness of the

Fig.7 Improvement in trench shape due to two-step annealing

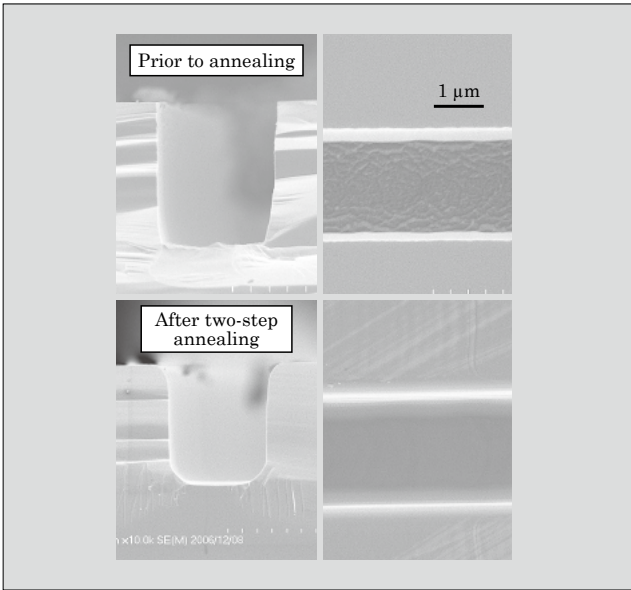
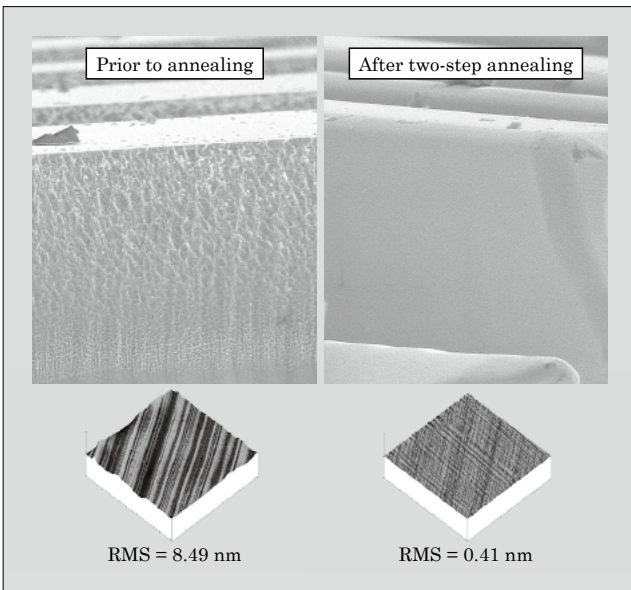


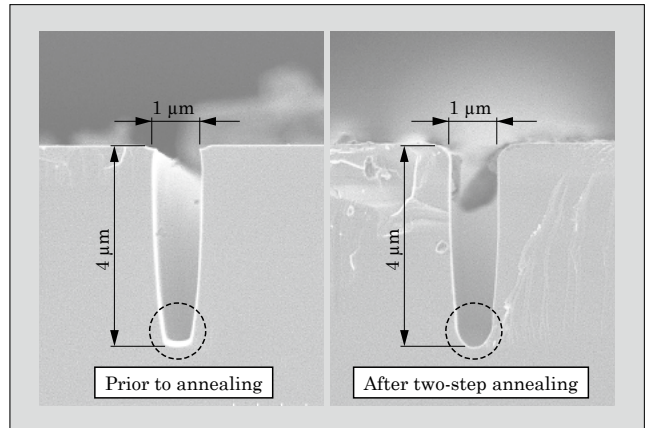
Fig.8 Improvement in trench sidewall due to two-step annealing



trench sidewall of a sample was evaluated both before and after performing two-step annealing with  $\text{SiH}_4/\text{Ar}$  and  $\text{H}_2$ , and the results are shown in Fig. 8.

The sample had a trench depth of  $8\text{ }\mu\text{m}$ , and the AFM analysis range was  $1\text{ }\mu\text{m}$  square. Prior to annealing, i.e., immediately after etching, a significant amount of roughness on the trench sidewall could be observed even when using a SEM. With the AFM, large surface unevenness was observed in stripe shapes, and the RMS value was  $8.49\text{ nm}$ . After annealing, the sample was smooth without any roughness that could be observed with the SEM. With the AFM, the extreme degree of smoothness was verified and the RMS value had decreased to  $0.41\text{ nm}$ . Thus, we were

Fig.9 Change in trench shape and dimensions before and after two-step annealing



able to verify that the two-step annealing process resulted in extremely smooth trench sidewalls.

### 3.7 Application of two-step annealing to small trenches

The effectiveness of two-step annealing on small trench sizes (widths) was also verified. Figure 9 compares the trench shape and trench size before and after two-step annealing.

We verified that a suitable roundness of the trench corners and a semicircular-shaped trench bottom were obtained without any change to the width or depth of the trench. As a result of these improvements, the trench shape compares favorably to that of a Si trench device.

## 4. Conclusion

We verified the effectiveness of high temperature annealing for improving the trench shape and inner wall smoothness of trenches formed by dry etching SiC material. By annealing at a pressure of 80 Torr and temperature of  $1,700\text{ }^\circ\text{C}$  in a  $\text{SiH}_4/\text{Ar}$  atmosphere, rounded trench corners and smooth inner walls of the trench could be obtained. However, surface roughness caused by step bunching occurred on the substrate surface. We also verified that annealing at a pressure of 80 Torr and temperature of  $1,500\text{ }^\circ\text{C}$  in a  $\text{H}_2$  atmosphere results in improved smoothness only, without any change to the trench shape. In order to realize both shape and smoothness improvements for a trench, we found that a two-step process of annealing in a  $\text{SiH}_4/\text{Ar}$  atmosphere followed by annealing in a  $\text{H}_2$  atmosphere enables improvements in the shape of trench corners, the smoothness of trench inner walls and the smoothness of the substrate surface. After the formation of a SiC trench, the implementation of annealing at a high temperature is believed to result in improved withstand voltage capability and electron mobility for a SiC-UMOSFET.

## Reference

- (1) Kuribayashi, H. et al. Investigation of Shape Transformation of Silicon Trenches during Hydrogen Annealing. *Jpn. J. Appl. Phys.* Vol. 43, no. 4A, 2004, p. L468-470.
- (2) Sudoh, K. et al. Numerical Study on Shape Transformation of Silicon Trenches by High-Temperature Hydrogen Annealing. *Jpn. J. Appl. Phys.* Vol. 43, no. 9 A, 2004, p. 5937-5941.
- (3) Karlsson, S., Nordell, N. AFM Study of In Situ Etching of 4H and 6H SiC Substrates. *Mater. Sci. Forum* vols. 264-268, 1998, p. L363-366.



### Explanation 4H-SiC

Silicon carbide (SiC) is known to take more than 200 polytypes (crystal forms). Research activities with practical interests have been focused on three polytypes, 3C-, 4H-, and 6H-SiC, due to their high probability in occurrence. Here, the initial numbers stand for the repetition period of unit cell along the c-axis, and the letters for the crystal system: C for cubic and H for hexagonal.

4H-SiC is most hopeful for power semiconductors, owing to its superior properties including approximately ten times as high breakdown field, three times as high bandgap, twice as high electron saturation velocity, and three times as high ther-

mal conductivity, as those of silicon. 4H-SiC has higher electron mobility and smaller anisotropy therein than 6H-SiC. Availability of high-quality single-crystalline wafers in recent years has opened employment mainly in power devices.

Polarity in SiC crystals provides two selections in using the {0001} plane: Si face and C face. Difference in crystal orientation is known to bring about, for example, different behaviors in epitaxial growth and different thermal oxidation rate. It is still under argumentation which face is more suitable for device fabrication.

# Main Businesses of Fuji Electric Group

## Energy & Electric Systems Group

Fuji Electric Systems Co., Ltd.

Fuji Electric FA Components & Systems Co., Ltd.

**Drives :** Drive control equipment, Drive systems, Power supplies, Rolling stock/  
Special machinery

**Automation :** Sensors, Measuring instruments, Controllers, Manufacturing solutions,  
Energy solutions, Social solutions

**Industrial plant engineering :** Industrial power supplies, Substation equipment for facilities,  
Substation equipment for electric railroads, Clean rooms

**Electric power systems :** Thermal power, Nuclear power, Hydraulic power

**Plant facility construction :** Electrical installation work, Air conditioning systems, Water supply/  
drainage installation work

**Electric distribution and control equipment :** Magnetic contactors, Manual motor starters (MMSs), Operation  
indicators, Molded-case circuit breakers (MCCBs), Earth-leakage  
circuit breakers (ELCBs), High-voltage vacuum circuit breakers, Low/  
high voltage fuses, Gas detectors, Energy management equipment

## Electronic Devices Group

Fuji Electric Device Technology Co., Ltd.

**Semiconductors :** Power MOSFETs, IGBT modules, Rectifier diodes, Power supply ICs,  
IGBT-IPMs, Pressure sensors

**Magnetic disks :** Aluminum media, Glass media, Aluminum substrates

**Imaging devices :** Photoconductive drums, Peripheral imaging devices

## Retail Systems Group

Fuji Electric Retail Systems Co., Ltd.

**Vending machines :** Various vending machine models

**Food service devices :** Assorted dispenser products, Tea servers, Refrigerated showcases

**Currency handling systems :** Coin mechanisms, Bill validators, Currency exchange machines,  
Automatic change dispensers, Coin mechanisms for leisure facilities,  
Non-contact IC card systems

**Cold-chain equipment :** Various types of store display cases, Store-related equipment, Store  
design, construction and maintenance services

# Global Network

## AMERICA

### ● FUJI ELECTRIC CORP. OF AMERICA

USA

Phone: +1-201-712-0555 Fax: +1-201-368-8258

### ◆ FUJI ELECTRIC DEVICE TECHNOLOGY AMERICA INC.

USA

Phone: +1-732-560-9410 Fax: +1-732-457-0042

## EU

### ■ FUJI ELECTRIC HOLDINGS CO., LTD.

Erlangen Representative Office

GERMANY

Phone: +49-9131-729613 Fax: +49-9131-28831

### ● FUJI ELECTRIC FA EUROPE GmbH

GERMANY

Phone: +49-69-6690290 Fax: +49-69-66902958

### ● FUJI ELECTRIC DEVICE TECHNOLOGY EUROPE GmbH

GERMANY

Phone: +49-69-6690290 Fax: +49-69-6661020

### ◆ FUJI ELECTRIC FRANCE S.A.

FRANCE

Phone: +33-4-73-98-26-98 Fax: +33-4-73-98-26-99

## ASIA

East Asia

### ■ FUJI ELECTRIC HOLDINGS (SHANGHAI) CO., LTD.

CHINA

Phone: +86-21-5496-3311 Fax: +86-21-5496-0189

### ■ FUJI ELECTRIC HOLDINGS CO., LTD.

China Representative Office (Beijing)

CHINA

Phone: +86-10-6505-1264 Fax: +86-10-6505-1851

### ● FUJI ELECTRIC FA (SHANGHAI) CO., LTD.

CHINA

Phone: +86-21-5496-1177 Fax: +86-21-6422-4650

### ◆ FUJI ELECTRIC (CHANGSHU) CO., LTD.

CHINA

Phone: +86-512-5284-5642 Fax: +86-512-5284-5640

### ◆ WUXI FUJI ELECTRIC FA CO., LTD.

CHINA

Phone: +86-510-8815-2088 Fax: +86-510-8815-9159

### ◆ FUJI ELECTRIC DALIAN CO., LTD.

CHINA

Phone: +86-411-8762-2000 Fax: +86-411-8762-2030

### ◆ FUJI ELECTRIC MOTOR (DALIAN) CO., LTD.

CHINA

Phone: +86-411-8763-6555 Fax: +86-411-8762-4077

### ● FUJI ELECTRIC MOTOR (SHANGHAI) CO., LTD.

CHINA

Phone: +86-21-5239-9681 Fax: +86-21-5239-9680

### ◆ SHANGHAI FUJI ELECTRIC SWITCHGEAR CO., LTD.

CHINA

Phone: +86-21-5718-1495 Fax: +86-21-5718-5745

### ◆ SHANGHAI FUJI ELECTRIC TRANSFORMER CO., LTD.

CHINA

Phone: +86-21-5718-1495 Fax: +86-21-5718-5745

### ◆ FUJI ELECTRIC SYSTEMS(SHANGHAI) CO., LTD.

CHINA

Phone: +86-21-5496-2211 Fax: +86-21-6417-6672

### ◆ DALIAN FUJI BINGSHAN VENDING MACHINE CO., LTD.

CHINA

Phone: +86-411-8730-5902 Fax: +86-411-8730-5911

### ● DALIAN JIALE VENDING MACHINE OPERATION CO., LTD.

CHINA

Phone: +86-411-8665-0277 Fax: +86-411-8596-2732

### ◆ HANGZHOU FUJI REFRIGERATING MACHINE CO., LTD.

CHINA

Phone: +86-571-8621-1661 Fax: +86-571-8821-0220

### ◆ FUJI ELECTRIC (SHENZHEN) CO., LTD.

CHINA

Phone: +86-755-2734-2910 Fax: +86-755-2734-2912

### ● FUJI ELECTRIC FA (ASIA) CO., LTD.

HONG KONG

Phone: +852-2311-8282 Fax: +852-2312-0566

### ● FUJI ELECTRIC DEVICE TECHNOLOGY HONG KONG CO., LTD.

HONG KONG

Phone: +852-2664-8699 Fax: +852-2664-8040

### ■ FUJI ELECTRIC SYSTEMS CO., LTD.

Taipei Representative Office

TAIWAN

Phone: +886-2-2501-1256 Fax: +886-2-2501-1250

### ● FUJI ELECTRIC TAIWAN CO., LTD.

TAIWAN

Phone: +886-2-2515-1850 Fax: +886-2-2515-1860

### ● FUJI ELECTRIC FA TAIWAN CO., LTD.

TAIWAN

Phone: +886-2-2370-2390 Fax: +886-2-2370-2389

### ◆ ATAI FUJI ELECTRIC CO., LTD.

TAIWAN

Phone: +886-3-321-3030 Fax: +886-3-321-7890

### ● FUJI ELECTRIC FA KOREA CO., LTD.

KOREA

Phone: +82-2-780-5011 Fax: +82-2-783-1707

## Southeast Asia

### ■ FUJI ELECTRIC SYSTEMS CO., LTD.

Bangkok Representative Office

THAILAND

Phone: +66-2-308-2240 Fax: +66-2-308-2242

### ■ FUJI ELECTRIC SYSTEMS CO., LTD.

Jakarta Representative Office

INDONESIA

Phone: +62-21-572-4281 Fax: +62-21-572-4283

### ◆ FUJI ELECTRIC (MALAYSIA) SDN. BHD.

MALAYSIA

Phone: +60-4-403-1111 Fax: +60-4-403-1496

### ◆ FUJI ELECTRIC PHILIPPINES, INC.

PHILIPPINES

Phone: +632-844-6183 Fax: +632-844-6196

### ● FUJI ELECTRIC SINGAPORE PRIVATE LTD.

SINGAPORE

Phone: +65-6535-8998 Fax: +65-6532-6866

### ● FUJI ELECTRIC FA SINGAPORE PRIVATE LTD.

SINGAPORE

Phone: +65-6533-0010 Fax: +65-6533-0021

■:Representative Office ●:Sales Base ◆:Manufacturing Base



